Auto-Zeroing Baseline Compensation for Chemical Sensor Signal Extraction

Sam McKennoch

A thesis submitted in partial fulfillment of the requirements for the degree of

Master of Science in Electrical Engineering

University of Washington

2002

Program Authorized to Offer Degree: Electrical Engineering

University of Washington
Graduate School

This is to certify that I have examined this copy of a master's thesis by

Sam McKennoch

and have found that it is complete and satisfactory in all respects,
and that any and all revisions required by the final
examining committee have been made.

Committee Members:

_____
Denise Wilson

_____
Bruce Darling

Date: _____

In presenting this thesis in partial fulfillment of the requirements for a Master's degree at the University of Washington, I agree that the Library shall make its copies freely available for inspection. I further agree that extensive copying of this thesis is allowable only for scholarly purposes, consistent with "fair use" as prescribed in the U.S. Copyright Law. Any other reproduction for any purposes or by any means shall not be allowed without my written permission.

Signature_____

Date _____

University of Washington

Abstract

Auto-Zeroing Baseline Compensation for Chemical Sensor Signal Extraction

Sam McKennoch

Chair of the Supervisory Committee:
Associate Professor Denise Wilson
Electrical Engineering

This thesis establishes auto-zeroing baseline compensation as a viable approach to stabilizing chemical sensor signal extraction. Baseline compensation ensures similar baseline and dynamic range at the output of the conditioning circuit, regardless of fabrication variation and sensor drift. These baseline compensation circuits are demonstrated in the context of processing resistance changes from composite-film polymer chemical sensors and tin-oxide chemical sensors and processing threshold voltage changes in ChemFETs. Because of the initial highly variable baseline state of chemiresistors and ChemFETs, a large number of bits in an A/D converter are required to translate the sensor information from an array of these sensors into a digital format for use by a microprocessor. In this work, a generic circuit is presented for auto-calibrating and compensating for the baseline of a variety of chemiresistive devices in order to improve concentration measurement resolution and analyte discrimination. The measurement circuits optimize sensor resolution via baseline compensation. The signal compensation technique is based on the governing transduction principles of the chemical sensor, thereby enabling signals to be compensated without distortion. Dynamic range is standardized to a constant regardless of initial baseline resistances. The resulting dynamic range can be as much as two orders smaller than an uncompensated circuit and achieve the same sensor accuracy. Simulations and experimental results indicate a factor of 68 improvement in resolution for typical A/D converter resolutions. In typical experiments, the described circuit exhibits half the response time to low concentrations of chemicals and over an 11% improvement in analyte discriminating ability versus uncompensated sensors.

Using the baseline compensation circuits, this thesis also describes a broad-base portable chemical discrimination module capable of using combinations of homogenous or heterogeneous arrays of chemical sensors for evaluating chemical type. Several types of sensors can be added to or removed from the system in plug and play fashion. Using these sensors, the module supplies the user with real-time chemical discrimination information. In addition to baseline compensation, additional signal processing is applied to homogenous sensor arrays to reduce the impact of corrupted sensors. Sensor outputs are displayed in principal component space in real-time, thereby enabling the user to evaluate the transient path of the sensors to their final posi-

tion in principal component space. Visual display of transient behavior is intended to improve usability in the field of these portable instruments.

TABLE OF CONTENTS

LIST OF FIGURES

LIST OF TABLES

CHAPTER 1 *Introduction*

Chemical Sensors are sensors that typically transduce information in the presence of chemicals into an electrical signal that can then be processed and interpreted for discrimination, concentration, and localization information. Many types of chemical sensors have been fabricated over the past forty years. They include conventional three electrode electrochemical configurations, FET-based sensors, QCMs (quartz crystal microbalances), and chemiresistors based on Conducting Polymers, Composite-Film Insulating Polymers and metal oxides. These sensors use a variety of transduction mechanisms and each have unique advantages and disadvantages that vary with application. As a cross-section of existing non-optical chemical sensors, this research effort has concentrated on using three types of chemical sensors, composite-film polymer chemiresistors, tin-oxide chemiresistors, and ChemFETs. More specifically, this research effort seeks to maximize extraction of the chemical sensor response signal using intelligent pre-processing and creative system integration. The techniques presented in this thesis are demonstrated on a representative set of chemical sensor technologies and can be used on a wide variety of optical and non-optical chemical sensing technologies.

SECTION 1.1 SENSOR OVERVIEW

Chemiresistors using composite-film insulating polymers, a relative recent addition to available chemical sensor technologies, show promise because of high sensitivity and linear response at low

chemical concentrations of interest. Linear response enables superposition while discriminating chemicals, greatly simplifying the resolution of analyte mixtures in the sensing environment. These sensors are also relatively inexpensive, are easy to manufacture, and are easily miniaturized for use in arrays of chemical sensors. Composite-film polymer chemiresistors are made of an insulating polymer matrix implanted with conductive particles, typically carbon-black [1]. Chemically induced swelling of the insulating polymer changes conducting paths through the carbon-black and thereby the resistance of the sensor. Large amounts of swelling produce a non-linear relationship with concentration, as predicted by percolation theory. For typical small-signal use however, these sensors demonstrate a change in resistance from baseline that is directly linearly proportional to concentration.

Tin oxide sensors are a member of the metal-oxide family of chemiresistors. The ease of fabrication of metal-oxide sensors along with their stability have made them popular in the commercial and research communities [2]. They react with reducing gases in the environment causing a change in sensor conductivity and resistance [3] [4]. A heating element helps to stabilize the thermal environment and improve sensor sensitivity. Resistance generally decreases from some baseline value with increased gas concentration. The nature of the input-output relationship in metal-oxide sensors is an inverse power law. A strong dependence on humidity has further been observed and characterized [3] [4].

ChemFETs are chemically sensitive field effect transistors. They are easy to integrate into support circuitry and are inexpensive. Chemically-sensitive gate materials cause the FET threshold voltage to change in response to certain analytes [5] [6]. Different types of chemFETs can be integrated onto the chip, including sensors that respond to a primary analyte and its interferents, in order to improve sensor discrimination capabilities. The nature of the input-output relationship between the channel voltage in a diode-connected ChemFET (in the saturation region of operation) and analyte concentration is logarithmic, providing increased resolution at low concentrations of analytes [6].

SECTION 1.2 SENSOR SIGNAL PROCESSING OVERVIEW

By the very nature of their heterogeneity, arrays of chemical sensors can exhibit a wide range of baseline values, types of outputs (resistance, voltage, etc.), dynamic ranges, and aging effects,

which impact system integration. Most of these parameters are artifacts of the manufacturing process used to make the sensors and provide little useful information on sensor response. For example, the wide range of initial baseline values if not compensated, leads to a very wide range of possible output values. This large dynamic range, once converted to digital values, causes a decrease in analyte concentration resolution because most of the dynamic range is consumed by baseline variation rather than by the sensor response to the analyte. Likewise, as many chemical sensors age, their baseline values tend to drift at rates of a few percent over a period of months, further compounding the dynamic range problem and adding further complexities to calibration. This research effort presents a viable solution to the problems of baseline variance and drift. Compensation methods are discussed which allow all sensors, regardless of the unknown initial baseline to be compensated to the same initial output value. Subsequent compensations over calibrated time periods are subsequently possible to decrease the effects of drift.

System integration of heterogeneous arrays of chemical sensors into an inexpensive, mobile chemical measurement unit requires consideration of many factors such as signal conditioning, the ability to flag broken sensors, and streamlining of signal processing for pattern recognition to suit portability. Signal conditioning is used to enhance data acquisition, which involves accurate analog to digital conversion of sensor data. In order to maximize the resolution of a mobile unit, baseline compensation can be used to fuse sensor signals in such a way that sensor dynamic range is reduced. Flagging broken sensors using statistical outlier removal techniques on homogenous arrays of sensors allows for a high degree of robustness to sensor failure.

In order to classify chemical analytes of interest, this work uses principal component analysis (PCA). Principal component analysis is a feature reduction method that transforms multiple-dimensional data into a vector space in which most variance is contained in the first few principal component directions. In highly correlated data, higher dimensional principal axes become less significant [7]. PCA has been used in chemical discrimination applications many times [8] [9]. In this work, PCA is used to reduce six-dimensional sensor data to two principal component dimensions. These dimensions are then displayed as an interface for the user to make classification decisions. This visual display decreases circuit complexity by using built-in human pattern classification abilities to make decisions regarding chemical detection based on the visual results

of PCA. PCA has been typically used as a visual aid in determining the discrimination capability of an array of chemical sensors and can be interpreted directly through visual observation, transferred to cluster analysis and discrimination factor analysis for linear signal processing, or used as a precursor in array design for more non-linear signal processing techniques.

Detection of analytes of interest in the presence of interferents is also an important topic of interest regarding chemical sensors. A simple integrated biologically-inspired circuit is discussed and evaluated in this research effort. When used in conjunction with the appropriate types of sensor arrays and with smart sensor-type choices, this circuit (used for interferent rejection) further increases the amount of information extracted from these sensors.

SECTION 1.3 CHEMICAL SENSING APPLICATIONS

For chemical vapor monitoring, a clear need exists for a low-power mobile chemical sensing platform capable of detecting a wide variety of chemical analytes and analyte concentrations. Potential applications include food monitoring (by detecting the outgassing components) [10], indoor air quality monitoring, and environmental monitoring. Chemical environmental sensing is particularly important in judging the impact that humans have on the environment. To be effective in the field, chemical sensing must be carried out in a real-time, distributed, and highly sensitive manner. By looking at the local effects of atmospheric pollutants, the causes and effects of atmospheric pollution on the regional and global scale can be better understood. Distributed chemical monitoring of atmospheric constituents could also potentially improve weather forecasting. In the case of chemical leaks, it might be useful to monitor the distribution gradient as the leak spreads in order to better contain it. A distributed network of the chemical sensors could allow industry to self-monitor or enable government to cheaply and efficiently monitor industrial pollution emissions in real-time.

Another category of applications for mobile, low-power distributed chemical sensing is in the area of indoor air quality monitoring. This category applies to office buildings, factories, and perhaps even the International Space Station. Currently air quality is being monitored through expensive, power-hungry techniques such as quadrupole mass spectrometry and ion mobility spectrometry. While these systems are indeed very accurate, distributed sensing holds many advantages. Due to

the inexpensive low-mass nature of distributed sensor arrays, a great deal of redundancy is possible. A properly optimized sensor array also has the capability to monitor more atmospheric constituents even before being routed into a computer for further analysis. With these sensors distributed throughout the structure, it would be possible to react to a leak or some other sort of detriment to the air quality in a very rapid and targeted manner. Intelligent pre-processing of the chemical sensor signals in essential to realize these schemes in order to reduce the effects of systematic and random variations within the sensors.

In addition, the recent events of September 2001 have made clear the need for accurate, distributed, low-power chemical monitoring. In order to better respond to potential acts of terrorism, the ability to detect potentially hazardous chemicals in a variety of places is extremely important because the time frame in which actions can be taken to counteract hazardous chemical attacks is extremely brief [11].

SECTION 1.4 ALTERNATIVE METHODS

A handful of research efforts have demonstrated techniques for improving portable instrument viability by reducing the inherent variation in chemical sensors with baseline compensation techniques. Standard methods using a wheatstone bridge cannot be applied because, for chemiresistors, the initial resistance varies across manufacturing and lifetime of the sensor. Apsel *et al* uses an adaptive, programmable amplifier to stabilize chemiresistors at a predetermined baseline value using floating gate analog memory and novel filtering techniques. The floating gate capability allows a continuous range of programmable values, theoretically enabling perfect baseline compensation (within the constraints of transistor performance); however, these circuits also contribute distortion to the sensor response, generating different response curves for the same analyte, same type of sensor, but different baseline resistances [12]. Using a different circuit design approach, Neaves and Hatfield have constructed an ASIC specifically designed to extract response signals from an array of polymer chemiresistors. This circuit results in fundamental distortion of the sensor signal by creating a non-linear response of the output current in relation to the input concentration. The ASIC is a versatile generic module for sensor resistance preprocessing, but contains bulky amplifiers and multipliers that may limit usefulness for large arrays in portable instruments in terms of space and power consumption [13].

Many other analyte recognition methods are available besides principal component analysis. For example, Brezmes et al. use two cascading artificial neural networks, each with one internal hidden layer [14]. The first neural network performs analyte identification while the second performs analyte quantification. The networks also take humidity as an input in order to decrease its effect on the measurements. While producing good results, this method lacks transparency in that the way in which the neural network makes the decision is not generally useful in helping the user determine the accuracy of the result. The results of the neural network are also highly dependant on the training data used [14].

As mentioned, the interferent rejection circuit employed in this effort helps to improve system selectivity to desired analytes by taking advantage of the effects of baseline compensation to eliminate interferents. Other efforts aimed at interferent rejection have tended to focus on improving sensor technology. For example, dopant amounts or operating temperature might be varied to alter selectivity [2]. This effort offers interferent rejection independent of sensor technology as variations in sensor technology have been compensated for.

One alternate approach to monitor chemical environmental impacts is via satellite observation. However, most earth-observing satellites acquire mainly image data. For example, the LANDSAT series of spacecraft acquires detailed images of various places around the world to be compared with earlier images in order to judge human impact and climate change. Images tell us little about the chemical composition of air on the ground level and the environmental impact that the chemical constituents of air can have. Other instruments such as the MOPITT (a gas correlation spectroscopy sensor) instrument on the TERRA satellite are optimized to detect only certain gases (carbon monoxide and methane in this case) and have limited spatial resolution (22km) [15]. Likewise, weather stations are not normally distributed in a very dense manner, depending on location. Also, weather stations are at the present limited in what data they collect (wind speed, temperature at various depths, and barometric pressure). In addition, weather stations are also limited to taking data at fixed points. Although, satellites and weather stations have very useful purposes, a clear need remains for a low-power mobile chemical sensing unit. Previous attempts to build such

devices have been limited by a number of factors such as power consumption, the need for a bulky computer to perform processing, and sensor technology issues like variable baseline and drift.

SECTION 1.5 NOVELTY

The following is a list of the novel components of this thesis:

- A series of discrete and integrated circuits are presented which use a mixed signal method for sourcing a constant current through a chemiresistor or chemFET in such a way that the sensor response is not distorted during compensation [16] [17].
- Due to the compensation mechanism used, as previously explained the baseline compensator is also able to act as a drift compensator. By limiting the dynamic range of a wide variety of sensor types all with different random and systematic variation, baseline and drift compensation help to enable more mobile low-power applications such as those listed above, all with distorting the sensor signal.
- The integrated circuit presented is the third in a series of integrated baseline circuits for different chemical sensor technologies that provides modular baseline-independent compensation with no distortion of chemical sensor signal. Advantages of the present integrated design over the discrete circuit include size (a factor of 1310 in reduced volume), cost (a factor of over 40 in reduced cost per compensated sensor), and accuracy.
- A biologically-inspired interferent rejection circuit is further shown to enhance the detection of primary analytes in the presence of closely-related interferents.
- The novel approach in this thesis to mobile chemical sensing uses intelligent pre-processing to enable effective principal component analysis. Human classification abilities can then be taken full advantage of by displaying PCA data for human interpretation as sensor responses approach analyte calibration clusters [18]. Similar work on system integration in the literature tends to concentrate more on odor localization and relies more on theoretical models for interpreting sensor data [19].

SECTION 1.6 THESIS ORGANIZATION

This thesis continues in Chapter 2 with a background on solid-state chemical sensors, including some of the inherent performance limits. The next chapter discusses multiple aspects of a family of circuits designed to overcome these intrinsic sensor problems. Chapter 3 also follows up the circuit design with circuit results, thereby directly demonstrating the ability of these compensation circuits to better extract chemical sensor information. Chapter 4 discusses the integration of the compensation circuit into higher-level systems and compares performance of these systems to other pre-existing chemical detection systems. Chapter 4 also suggests possible areas of research that could use this effort as a starting point, and finally summarizes the main points and results of this research effort. The circuit and system integration results demonstrate the ability of the presented circuits to greatly enhance the minimum analyte detection resolution and ability to discriminate between analytes.

CHAPTER 2 *Background*

As discussed briefly in the introduction, chemical sensors present many challenges to efficient signal extraction. This chapter begins with a more detailed background on the three sensor technologies used to demonstrate the circuits in this research: (a) composite-film polymer sensors, (b) tin-oxide chemiresistors, and (c) chemical field effect transistors (ChemFETs). Following the sensor descriptions is a detailed analysis of some of the problems associated with successful signal extraction including the processing of noise, baseline variance and drift.

SECTION 2.1 COMPOSITE-FILM POLYMER CHEMIRESISTORS

Composite-film polymer chemiresistors are a recent entry into the field of chemical sensors. They have many advantages including that they are inexpensive and easy to manufacture. Composite-film chemical sensors are chemiresistors made of organic (insulating) polymers implanted with conductive carbon-black particles. The polymers in the sensors swell reversibly in response to vapor exposure due to analyte adsorption. Using different organic polymers in different combinations in the manufacture of these sensors, this type of chemiresistor can be made responsive to different types of analytes to varying degrees. When a chemical is applied to which the sensor is to some degree sensitive, the polymer swells. In swelling, the deposited carbon-black particles are forced to move farther apart, thereby changing the effective conductivity of the sensor [9]. This

change in conductivity can be measured as a resistance and correlated to chemical vapor concentration.

Figure 2-1 shows the behavior of these types of chemiresistive sensors when the initial volume percentages of the conductor carbon-black is varied. In general, it has been observed that two processes, diffusion and percolation, enable a fluid to move through a disordered medium. In the composite polymer film chemiresistor, the process of percolation dominates diffusion, due partially to the fact that it is possible for particles to become trapped in the sensor lattice. In diffusion, the probability that a particle will move either to the one side or the other is non-zero, whereas in percolation, once a particle becomes trapped, this probability can become zero. This observation affects the transduction properties of the sensor. In general, the process of percolation helps to

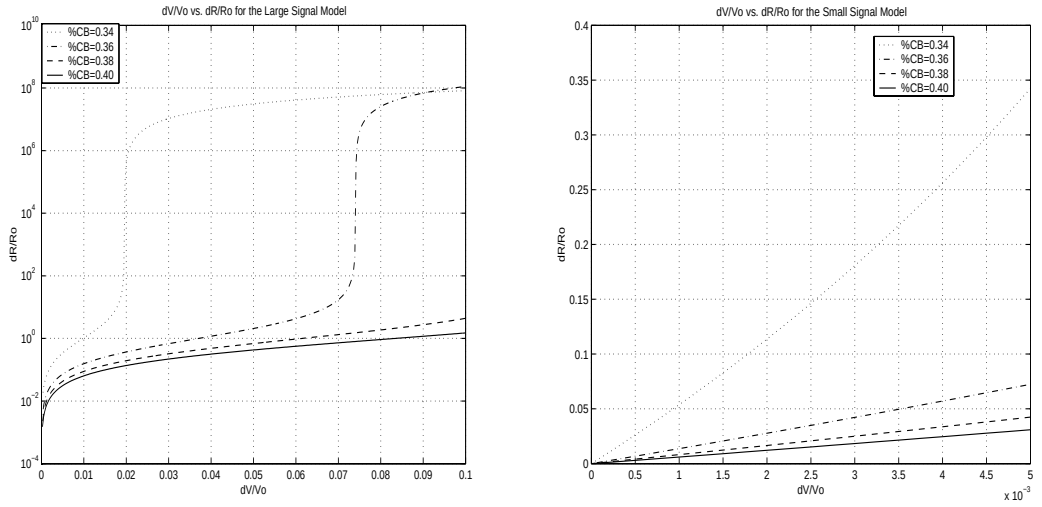

(a) (b)

FIGURE 2-1. Large and Small Signal Models of Carbon-Black Insulating-Polymer Sensors

The curves demonstrate the relationship between the sensor resistance and the change in sensor volume caused by an analyte. %CB represents different initial amounts carbon-black volume fraction. The sharp increases in dR/Ro at %CB= .34 and .36 in (a) are due to the sensor passing through its percolation point, i.e. this is the point (not accounting for electron tunneling) at which there are no longer any conduction paths through the insulating matrix and the resistance of the sensor begins to resemble the resistance of the insulating polymer itself [20]. Note that the small-signal model in (b) is approximately linear with an rms error from a true linear relationship of 0.0053 percentage change in resistance.

relate the swelling of the sensor as caused by an absorbing analyte to the change in its conductivity. Initially the resistance of the sensor resembles that of the conductor carbon-black, but as swelling occurs and conduction paths through the carbon-black decrease, the sensor resistance then approaches that of the insulating polymer. A sharp threshold called the percolation threshold occurs at which all conduction paths through the carbon-black have disappeared, leading to a sharp transition in resistance [20] [21]. Assuming only two discrete conductances possible in the sensor (that of the carbon-black and that of the insulating polymer) a formula for the relationship of the volume fraction of carbon-black particles to resistance across the composite film may be quantified using a binomial probability distribution as:

$$R = \left(\frac{L}{A}\right)\frac{(z-2)\rho_c\rho_m}{B + C + [(B+C)^2 + 2(z-2)\rho_c\rho_m]^{1/2}} \quad \textbf{(Eq 2.1)}$$

$$B = \rho_c[-1 + (z/2)(1 - (v_c/f))] \quad \textbf{(Eq 2.2)}$$

$$C = \rho_m[(zv_c/2f) - 1] \quad \textbf{(Eq 2.3)}$$

L is the length of the sensor resistor; A is the cross-sectional area of the sensor resistor; z is the number of conductances connected to each node in the lattice, also known as the coordination number; f is the packing factor. It ranges from 0.52 for simple cubic spheres to 1 for maximum packing. ρ_c is the resistivity of the carbon-black particles while ρ_m is the resistivity of the insulating polymer. The input to the equation is v_c, the volume fraction of carbon-black particles. Many other factors have also been known to affect swelling and likewise resistance changes including temperature, humidity, pressure, and electron tunneling [20] [21]. The percolation properties of composite-film sensors help to create highly-sensitive sensors that are responsive to many different types of analytes. However, the added complexity in the manufacturing of these sensors compared to simple conducting polymer sensors allows for more systematic and random manufacturing variations; thus, the initial baseline resistances of this type of sensor covers a broad range and is dependent on such factors as the type of insulating polymer used, and the initial volume fraction of carbon-black, thus making transduction of the sensor signal to a useable form difficult.

The sensor response becomes less and less reversible as it is pushed beyond the percolation threshold. Normally, these sensors would be operated at low chemical concentrations where there is a

fairly linear relation between the chemical concentration and sensor resistance. The small-signal response of this type of sensor may be characterized by [22]:

$$\frac{\Delta R}{R_o} = k[C] \qquad \textbf{(Eq 2.4)}$$

R_o is the baseline sensor resistance; ΔR is the change in resistance from the baseline; *[C]* is the applied vapor concentration, typically in ppm; *k* is a sensor constant. This equation demonstrates that the baseline value of resistance does not affect the slope of the response curve, as only *k* affects the slope. *k* may change with % Carbon-Black and polymer film thickness, but these factors are not considered here. *k* does depends on the chemical applied and the type of polymer being used. Examples of the value of *k* are 0.00004 PPM^{-1} with the polymer poly(ethylene oxide) and applied chemical cyclohexane, and a value of 0.0008 PPM^{-1} with the polymer poly(carbonate bisphenol A) and applied chemical toluene [22].

SECTION 2.2 TIN-OXIDE CHEMICAL SENSORS

Tin-oxide chemiresistors, unlike composite-film polymer chemiresistors and ChemFETs have been commercially available for some time, and are arguably responsible for saving lives in Japan by alerting users to potentially dangerous natural gas leaks. Tin-oxide is an n-type semiconducting metal oxide whose conductivity properties are highly sensitive to gases present in the environment. The primary reaction in the sensor to analytes is a reduction one, although chemisorption has also been shown to have an effect [3]. In the redox reaction, oxygen in the environment first interacts via dangling bonds with the sensor surface or grain boundary, extracting electrons and thereby creating a substantial depletion region [2]. Reducing gases in the environment then combine with oxygen in the thin film to enable the change in sensor conductivity and resistance by reinjecting electrons and decreasing the depletion region [3] [4]. It is important that oxygen saturates the sensor prior to introduction of a reducing gas in order to isolate the two effects. In part, because of this non-selective reaction to reducing gases, tin-oxide chemiresistors exhibit poor selectivity. These sensors do, however, show excellent stability, are fairly straightforward to fabricate and are moderately compatible with standard IC fabrication methods [2].

Other issues associated with tin-oxide sensors include sensor response speed and sensitivity to temperature. When an analyte is applied, response speeds vary with chemical concentration. The higher the analyte concentration, the faster the response because the oxygen on the film is combined with more quickly. This reduction in response time can reduce the response time from several minutes to only seconds. However, when the analyte is removed, the response time to return steady-state is constant because the partial pressure of oxygen is constant [3].

Due to the transduction mechanism employed by tin-oxide sensors, sensitivity to different analytes is highly dependant on sensor temperature. The sensors employed in this research effort maintain a constant temperature by using a heater filament, thus also stabilizing sensitivity to analytes. This stability comes at the cost of increased power consumption as a large amount of power is dissipated as heat.

The input-output equation may stated as below:

$$\frac{1}{R} = \frac{1}{R_o} + a[C]^r \qquad \textbf{(Eq 2.5)}$$

a is a sensitivity coefficient; *r* is a power law exponent for oxides. A strong dependence on oxygen partial pressure and humidity has further been observed and characterized [3] [4]. For oxygen partial pressure:

$$\frac{1}{R} \propto P_{O_2}^{-0.5} \qquad \textbf{(Eq 2.6)}$$

In the case of humidity, water vapor in the air has been shown to act as an electron donor gas, forming surface hydroxyl groups, thus decreasing sensor resistance. Humidity affects sensitivity to different analytes differently due to the way various analytes and water vapor react [3].

Although these sensors are much more widely used, problems with signal extraction has limited their commercial largely to binary triggers of toxic gas levels. As discussed above, the initial baseline resistance and subsequent drift of these sensors is highly effected by many environmental parameters such as humidity and temperature, thus creating difficulty in reliably and consistently extracting the chemical sensor signal.

SECTION 2.3 CHEMFET CHEMICAL SENSORS

ChemFETs are a member of FET based chemical sensors that also includes ISFETs (Ion-selective FET) and ENFETs (enzyme FET). Unlike ISFETs and ENFETs, ChemFETs have a conductive gate, thereby eliminating the need for a large reference electrode and enabling ChemFETs to be more easily integrated and miniaturized into support circuitry [2]. The gate material, generally a heavily-doped conducting polymer, is applied on a standard gate oxide. When a chemical is applied to which the gate material is sensitive, the fermi level at the gate shifts causing a change in the work function of the metal changes via bulk and surface modulation thereby causing the threshold voltage of the FET to change in a measurable way [5] [6]. Typically, ChemFETs are diode-connected as shown in Figure 2-2 where the gate is hardwired to the drain. This connection

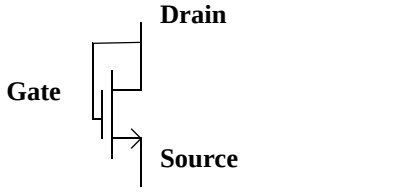

FIGURE 2-2. A diode-connected ChemFet

helps ensure that the transistor is in the saturation region of operation so long as the gate to source voltage is greater than the FET threshold voltage. Although research continues to define the fundamental behavior of the ChemFET, the basic input-output relationship of a diode-connected ChemFET with a constant drain-source current applied can be modelled as:

$$V_o = x_o \ln(a[C]) + x_1 + \sqrt{\frac{2I_D}{k'(W/L)}} \qquad \textbf{(Eq 2.7)}$$

x0 and *x1* are constants which depend physical device parameters associated with the materials used to build the ChemFET and the geometry of the device as well. They do not change in a meaningful way in response to an applied analyte and can be determined empirically. a is a scaling factor. *[C]* is the concentration of the analyte; I_D is the drain current through the ChemFET. It is generally set to some constant value during signal extraction. *k'* is another physical parameter dependent on the per unit area gate capacitance and electron mobility in the device; *W* and *L* are the width and length of the FET channel. The nature of the input-output equation is then logarith-

mic. However, this formula is only valid for a certain range of concentrations, a moderate range where at certain concentrations above and below this range the above relationship does not apply [6]. Figure 2-3 shows initial verification of this input-output relationship model for a ChemFET. The relationship between output voltage and the log of analyte concentration is approximately linear over a broad middle range of concentrations as expected.

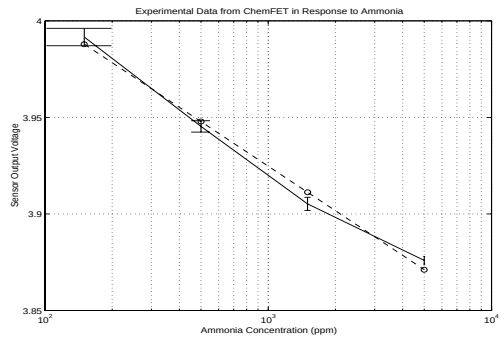

FIGURE 2-3. Experimental ChemFET Data

Preliminary verification of theoretical ChemFET model using 961 measurements at each of four different ammonia concentrations, 150, 500, 1500, and 5000 ppm. RMS error of the predicted best-fit line is 3.7 mV.

A further factor affecting compensation in the case of the ChemFETs is the transient settling time. For the purposes of this discussion, settling time is the time it takes for the ChemFET to arrive to within 0.1% of its final value after a constant current has been applied through it, in the absence of any analyte. A regular FET of this size should have a settling time of a maximum of a few nanoseconds [23], however certain peculiarities of the ChemFET fabrication process tend to greatly extend the settling time. In the fabrication of typical Aluminum-gate MOSFETs the final step is to anneal the aluminum, however this step cannot be performed in ChemFETs due to the modified gate materials used, instead ChemFETs must be allowed to fully warm up to counteract this initial drift. Settling times on the order of many minutes have been observed.

ChemFET technology is still being adjusted to produce more robust sensors. One of the current problems associated with fabrication, the transient settling time, creates problems in that the range

across which the sensor settles creates an enlarged sensor dynamic range, thus reducing the resolution to which analytes might normally be measured.

SECTION 2.4 CHEMICAL SENSOR NOISE

All sensing systems experience noise of various types. Noise is an important factor affecting chemical sensor behavior, because transduction relies on an actual chemical surface reaction. This reaction is by nature a random process and therefore subject to noise. In certain cases noise information can be useful, and may even be an indicator of sensor health [24]. However, in general, noise serves to limit the resolution to which analyte resolution can be measured by increasing the uncertainty in measurements. It is therefore important to understand how noise affects various types of chemical sensors before presenting a solution. The following is a discussion of various noise types that exist in the context of how they affect the sensors described here.

Thermal Noise: Thermal noise is caused by the random motion of electrons in response to thermal excitation and applies to all materials operating above $0°K$. This form of noise is especially troublesome in resistors because resistors tend to be high consumers of power which generates heat thereby increasing electron thermal velocity and the associated thermal noise. Thermal noise is independent of frequency of operation [25]. For resistors, the rms value of the thermal noise may be calculated as:

$$\overline{v^2} = 4kTR\Delta f \qquad \textbf{(Eq 2.8)}$$

k is boltzman's constant; T is the temperature is degrees Kelvin; R is the resistance value; Δf is the bandwidth of the circuit into which the sensor is placed. For example, an rms noise voltage value for a $100k\Omega$ resistor at room temperature in a circuit with a 10MHz bandwidth is $129\ \mu V$. In chemiresistors the dominant noise type is thermal [9] [26].

Shot Noise: Shot noise arises due to the fact that current is not a continuous rate of flow of carriers; a single electron has a finite amount of charge. This discrepancy between a discrete and a continuous flow is especially noticeable at low frequencies. Bipolar junction transistors exhibit high amounts of shot noise. This high amount of noise is present because the time of arrival of carriers as they diffuse and drift to the collector-base junction is a random process. For a bipolar junction

transistor in a circuit of bandwidth 10MHz and base current of 100mA, the rms current noise is 0.57 μA. Shot noise is also present in field-effect transistors, such as ChemFETs, but is only associated with the gate leakage current and can be neglected relative to more dominant types of noise because the gate leakage current in MOS devices is very near zero [25]. Shot noise therefore does not play a large role in the types of chemical sensors considered here.

Flicker Noise: Flicker noise is also known as 1/f noise, because it exhibits an inverse relationship with frequency. This type of noise is caused by the interaction of electrons with surface and interface states where electrons can sometimes become trapped for longer periods of time than elsewhere in the material. This trapping mechanism produces noise at frequencies typically below a few kHz, although this boundary can be much higher. Flicker noise is a particular problem in field effect transistor structures, because electrons are accelerated through a high electric field through the channel of the transistor and electron traps in the interface between the channel and insulating layer between channel and gate have a significant effect on the net flow of electrons through this shallow channel underneath the gate. Device constants used in the calculation of flicker noise can vary greatly due to random crystal imperfections associated with the manufacturing process. For a FET with a DC drain current of 1mA, operating frequency of 1kHz, and circuit bandwidth of 1MHz, the rms drain current noise due to flicker is approximately 1μA rms [25].

Burst Noise: Burst noise is low frequency noise. It is not fully understood and may be correlated with heavy-metal ion contamination. This type of noise can cause hump-like protrusions in the frequency spectrum. The method of production used determines whether this noise is present. This type of noise does not appear to play a large part in the types of sensors discussed here [25].

Avalanche Noise: Avalanche noise occurs in zener diodes and avalanche junctions. This type of noise is caused when carriers in a highly reversed-biased pn junction gain sufficient energy to cause impact-ionization and thereby produce more carriers through electron-hole generation. It does not generally play a role in resistors or FETs [25].

Specifically for FETs the noise can be modeled as a combination of thermal and flicker contributions:

$$\overline{i_d^2} = 4kT\left(\frac{2}{3}g_m\right)\Delta f + K\frac{I_D^a}{f}\Delta f \quad \textbf{(Eq 2.9)}$$

$$g_m = k'\frac{W}{L}(V_{GS} - V_t) \quad \textbf{(Eq 2.10)}$$

K is a device constant determined by contamination and crystal imperfections; *a* is a constant that varies from 0.5 to 2; *k'* is a device constant associated with geometry and doping; *Vgs* is the gate to source voltage of the FET; *Vt* is the threshold voltage of the FET. There is noise in the gate leakage current also (shot noise), but because it is so small, it can be ignored in most cases. According to these equations, the noise present in a ChemFET should be greater than a regular FET because W/L is larger, and I_d can be into the mA range. This discrepancy is noise level has been observed. In a JFET, part number MPF102, operating under identical conditions, the noise level was observed to be less than half that of the ChemFET. Besides changing the device itself, from this equation, one could lower the temperature, decrease the circuit bandwidth, or increase frequency. Note, that due to the presence of the threshold voltage in this equation, that the noise varies with the work function (and therefore chemical modulation). In general however, noise in ChemFETs in less than that of chemiresistors.

SECTION 2.5 CHEMICAL SENSOR BASELINE VARIANCE

Many chemical sensors that physically interact with the environment are subject to wide fluctuations in baseline output in part due to the inability to control surface characteristics during the fabrication. Surface characteristics are notoriously difficult to control during microfabrication and in most electronic devices, the signal due to surface characteristics is minimized. In chemical sensors, however, it is the surface that provides the bulk of the sensor signal in response to chemical changes in the sensing environment. In order to acquire a useful response of the sensor then, the surface must be a significant part of the overall electronic signal in comparison with the bulk. This catch 22 of chemical sensor fabrication results in large variations in baseline characteristics for good chemical sensors. In many chemical sensing systems, variations in baseline are not compensated and subsequently consume a large part of the resolution of the subsequent signal processing electronics. The straightforward, brute-force solution to this problem is to increase the resolution of the signal processing electronics to a number of bits that accommodates the range of baselines

generated by fabrication variations and the required resolution within the sensor response itself. A more elegant solution is to compensate for these baseline variations during signal preprocessing so that subsequent analog-to-digital converters in the signal flow focus their resolution capability on the sensor response itself. Achieving accurate, robust baseline compensation is one of the main objectives of this research effort. Baseline compensation reduces the range of the inputs extracted from these arrays into a more uniform set in such a way that the capabilities of the electronic signal acquisition are focused on the actual signal range rather than on artifacts of the sensor transduction. For a well designed chemical sensing system, baseline variation should be removed from the signal as early in the signal processing stream as possible. This effort seeks to remove baseline variation as part of the signal extraction from the sensor rather than during subsequent post-processing, thus ensuring the most accurate baseline compensation possible.

SECTION 2.6 CHEMICAL SENSOR DRIFT

Initial, wide baseline variation is compounded by sensor drift over time and other aging factors. Drift can be caused in part by the incomplete release of analyte vapor after an experiment has ended. Drift rates noted in experiments are generally limited to a 3% percent increase from the original baseline value over the period of a week. In experiments done elsewhere on composite film polymer chemiresistors, drift rates of approximately 16% were observed over a 3 month period.

Drift does not strongly affect the sensor sensitivity and if compensated, will have only a negligible effect [9]. Because the rate of chemical sensor drift in general is much slower than the rate of chemical sensor reaction to an analyte, a baseline compensator need only recompensate the sensor periodically to maintain a near-constant baseline value in the absence of an analyte. This recompensation can be done in real-time using a baseline compensator circuit and pre-calibrated drift rates. Compensation changes the problem to one of optimizing the drift reset frequency in the software, which is easily changed to accommodate a wide variety of situations. Drift compensation further limits and standardizes sensor dynamic range, thereby preventing a loss in system resolution due to drift. The baseline compensator developed in this thesis is shown to be an effective drift compensator as well.

The three types of chemical sensors chosen for this research effort have vastly different dynamic ranges and transduction mechanisms, making it significantly more difficult to use these sensors together in heterogeneous arrays of sensors for mobile applications. Other problems such as baseline variance, drift, and noise further compound the successful use of these sensors. Subsequent chapters will further elaborate on solutions to the problems presented here through the design of an auto-zeroing baseline compensation circuit.

CHAPTER 3 *Circuit Design and Experimental Results*

This chapter discusses the evolution of a circuit designed to compensate for variable sensor manufacturing variability and drift as well as other non-desirable variations in sensor responses. More specifically, the following topics are discussed in this chapter: (a) baseline compensation, (b) outlier detection and removal, and (c) interferent compensation. Three different baseline compensation circuits are presented and compared against one another using quantitative and qualitative experimental results. The discussion of outlier removal and interferent compensation emphasizes the ways in which baseline compensation enables other types of signal processing that can further enhance the information extracted from chemical sensors.

SECTION 3.1 BASELINE COMPENSATION CIRCUIT REQUIREMENTS

Standard methods using a wheatstone bridge are not well-suited to baseline compensation. For example, the Wheatstone bridge requires the bridge to be initially balanced before a change in resistance can be effectively measured. In addition, the sensitivity (the change in the output given a fixed change in the input) is not constant, especially for large deviations from baseline [27]. Although not necessary, a constant sensitivity is a desirable trait. Likewise, for the ChemFET, the circuit must be capable of dealing with a range of initial FET threshold voltages and a slightly variable width and length of the FET itself. In the end, in a hybrid system, preprocessing modules must

transform each type of sensor signal into one that has similar dynamic range and speed limitations for subsequent processing.

In addition to the above requirements, the circuit should be capable of interacting with the three types of sensors used in this research effort, Composite-film polymer chemiresistors, Tin-Oxide chemiresistors, and ChemFETs. The circuit should also implicitly be able to compensate the wide range of sensor characteristics within each sensor technology. In the case of the tin-oxide sensors and composite-film polymer chemiresistors, the circuit must be capable of measuring a small change in resistance over a large, but unknown initial resistance. A series of circuits are presented that meet these needs through various types of feedback, to adapt to changing initial sensor conditions.

SECTION 3.2 MANUAL AUTO-ZEROING BASELINE COMPENSATOR

In order to provide proof-of-concept for auto-zeroing baseline compensation, a discrete circuit has been constructed to provide manual-zeroing baseline compensation. Although this circuit can be used on any of the three types of sensors discussed here, it has been primarily tested using ChemFETs by researchers (Janata et. al.) investigating sensor properties at the Georgia Institute of Technology. This circuit performs all the same functions as an auto-zeroing baseline compensator except that it is necessary to manually adjust a potentiometer for each compensation.

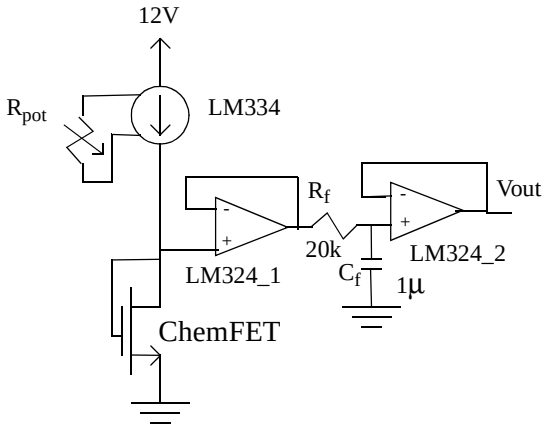

FIGURE 3-1. Manual-Zeroing Baseline Compensation Circuit Schematic

Figure 3-1 shows the schematic of the manual-zeroing baseline compensation circuit. This circuit uses a commercially available discrete variable current source, the LM334. A constant current is injected into the diode-connected ChemFET, such that the ChemFET is biased at some constant baseline voltage above threshold, typically 5V. At room temperature, the injected current is controlled by the potentiometer as:

$$I = \frac{0.067}{R_{pot}} \qquad \textbf{(Eq 3.1)}$$

The sensor output voltage is then buffered, passed through a low-pass filter and buffered again en route to a data acquisition system. The buffers prevented loading effects from changing the operating characteristics of the circuit. The low-pass filter employed is a simple RC filter with a cut-off frequency of approximately 8 Hz. Figure 3-2 shows the frequency response of this filter. Viable signals from the ChemFET have been found to normally change at a rate less than a few hertz and so this filter has the desired effect of reducing high-frequency noise. This circuit is simply meant to show that the baseline output voltage of the sensor circuit can manually be driven to a constant and uniform value by modulating the current source. The current then remains constant, but subsequent changes in the sensor properties as caused by an applied analyte then cause the output voltage to deviate from its baseline value in a predictable way, according to the transduction relationships presented in Chapter 2.

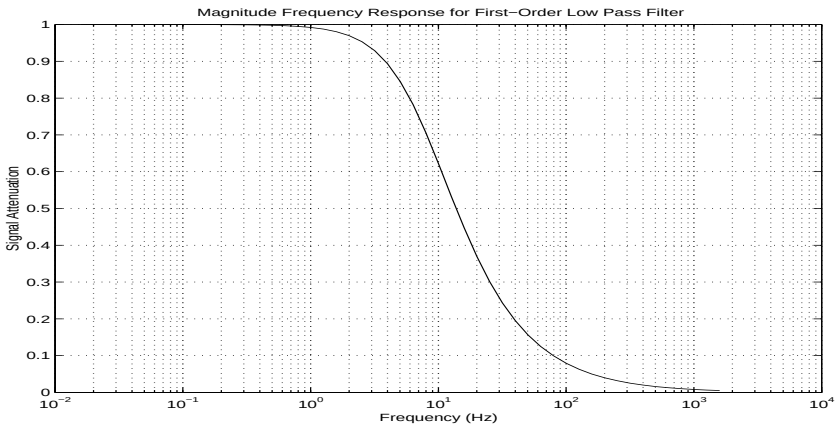

FIGURE 3-2. Magnitude Frequency Response for a First-Order Low Pass Filter

The cutoff frequency is 8 Hz. The magnitude rolls off at 20dB/decade.

Because the ChemFET requires high currents, typically in the mA range to operate, self-heating is a possible effect that can change the current regulation properties of the LM334. A more accurate formula for the output current including temperature effects is:

$$I = \frac{227 \cdot 10^{-6}}{R_{pot}} \cdot T(^{\circ}K) \qquad \textbf{(Eq 3.2)}$$

To alleviate performance problems caused by temperature variations, an additional heat sink has been placed on the LM334. However, the settling effects of the ChemFET dominates those of the LM334. Due to fabrication issues associated with the ChemFET, ChemFETs should be allowed to settle thermally for a period of several minutes. The LM334 will settle into its thermal environment long before the ChemFET. Because the output current required for ChemFETs is several milliamps, the final output current of the LM334 may differ from that expected due to temperature effects, however, the most important consideration is that the output current be constant regardless of the actual value. The LM334 does produce a constant output current, even under thermal loading conditions.

SECTION 3.3 VARIABLE-RESISTOR AUTO-ZEROING BASELINE COMPENSATOR

Having demonstrated the usefulness of baseline compensation, the next step is to automate the compensation. This auto-zeroing eliminates the effects of sensor manufacturing variability and drift through automatic compensations, thus allowing the user to concentrate on interpreting sensor outputs rather than extracting the signal itself. In the case of chemiresistors, many ways to extract the resistance signal from each sensor are possible. The simplest circuit possible is the voltage-divider, in which a voltage supply can be placed across two resistors. The output voltage is tapped at the joining of the two resistors, where one of the resistors is the chemiresistive sensor. However, voltage dividers suffer from many drawbacks. For the purposes of sensing applications, sensitivity may be defined as the amount a measurement circuit output changes for a fixed change in the sensor state. Voltage dividers have a highly non-linear sensitivity, and especially poor sensitivity to small changes in sensor state. In the case of chemical sensors, small changes in sensor states can be very important. The voltage divider therefore, despite its simplicity, is not a desirable choice for a compensation circuit.

Traditionally, a slightly modified voltage divider called the Wheatstone Bridge shown in Figure 3-3 has been used successfully to measure small changes in sensor resistance in the presence of large baseline resistances. The sensitivity of this circuit is approximately constant for small changes in sensor resistance [27]. The wheatstone bridge serves as the basis for the next design used to per-

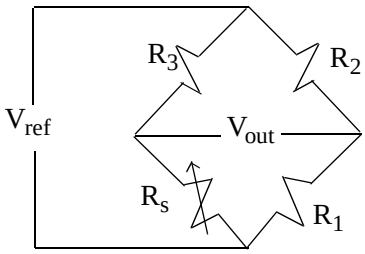

FIGURE 3-3. Wheatstone Bridge

form baseline compensation. However, in order for a wheatstone bridge to work properly it must be initially balanced so that R_3=R_S, where R_S is the sensor to be measured. A method to achieve this result is to initially adjust R_3 until the circuit output is zero. The variable-resistor auto-zeroing baseline compensator accomplishes this result by way of a feedback circuit shown in Figure 3-4.

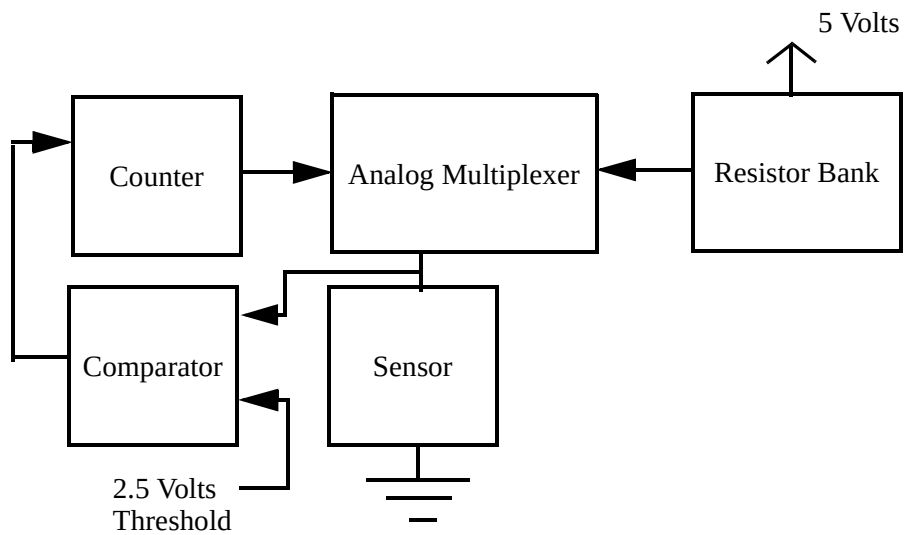

FIGURE 3-4. Variable Resistor Auto-Zeroing Baseline Compensator Compensation Scheme

The feedback circuit uses two stages. Stage one performs rough compensation by matching R_3 to within $10k\Omega$ of R_S. The second stage then matchs R_3 to within $1k\Omega$ of R_S. Each stage is enabled when a counter is reset and begins to count up. The output of the counter is connected to an analog multiplexer. The analog multiplexer is connected to series of resistors of different values, as well as to the sensor resistance. A comparator is used to determine when each compensation stage has finished.

This method of resistor matching to achieve compensation is highly approximate at best. The initial range of possible baseline resistances is quite large, and so in order to keep the resistor bank from growing to an unreasonable size, a certain amount of resistance matching error must be accepted, hence the sensor is only matched to the nearest $k\Omega$, and only a limited range of baseline resistances are able to be compensated. In order to provide a numerical comparison between the accuracy of this circuit and of those to follow, measurements have been taken to determine compensation accuracy. Table 3-1 below summarizes the results. The average compensation error is 45mV.

Table 3-1 - Measured vs. Ideal Baseline Outputs for Variable-Resistance Compensation

Baseline Resistance	Compensated Voltage	Ideal Output Voltage	Absolute Difference
$20k\Omega$	Out of Range	0V	Out of Range
$50k\Omega$	0.046	0V	46mV
$70k\Omega$	0.035	0V	35mV
$110k\Omega$	0.054	0V	54mV
$200k\Omega$	Out of Range	0V	Out of Range

While the compensation error limits for this circuit are small to provide accurate baseline compensation over a limited range, and certainly comparable to the capabilities of other types of compensation circuits, other drawbacks prevent its widespread use for chemical sensor signal processing. First of all, this circuit is not capable of being used with non-chemiresistive sensors such as ChemFETs because it is a resistance matching scheme. Although a resistor attached between the ChemFET source and V_{dd} could be used as a current source to bias the ChemFET, as the ChemFET

threshold voltage changes, the voltage across the resistor changes thus changing the bias current. This type of current source is therefore not constant and serves only to complicate the process of signal extraction.

Secondly, the range of this circuit is limited, in this case to 169kΩ, because of the limited number of bits on the analog multiplexers. In the case of the results in Table 3-1 resistances 20kΩ and 200kΩ are out of range because either the first or second stage fails when compensation is attempted on them. For example, in the case of the 20kΩ resistor, the circuit has been setup to count from 30kΩ to 190kΩ in increments of 10kΩ and so 30kΩ is sufficient to trigger the first stage to stop. The second stage then begins to count down in 1kΩ increments. Due in part to the additional on-resistance of the analog multiplexer, the circuit is not able to count down to a resistance of less than 20kΩ, and so the second stage fails in compensation.

Further problems with this circuit include the fact that this compensation scheme is not easily integrated because of the heavy emphasis on resistive circuits. Also, as alluded to previously, the on-resistance of the analog multiplexer slightly distorts the compensation process and limits the resistance resolution to which compensation can occur. The analog multiplexers used in this circuit has on-resistances that vary from approximately 50Ω to 500Ω. Lastly, as Figure 3-5(b) demonstrates,

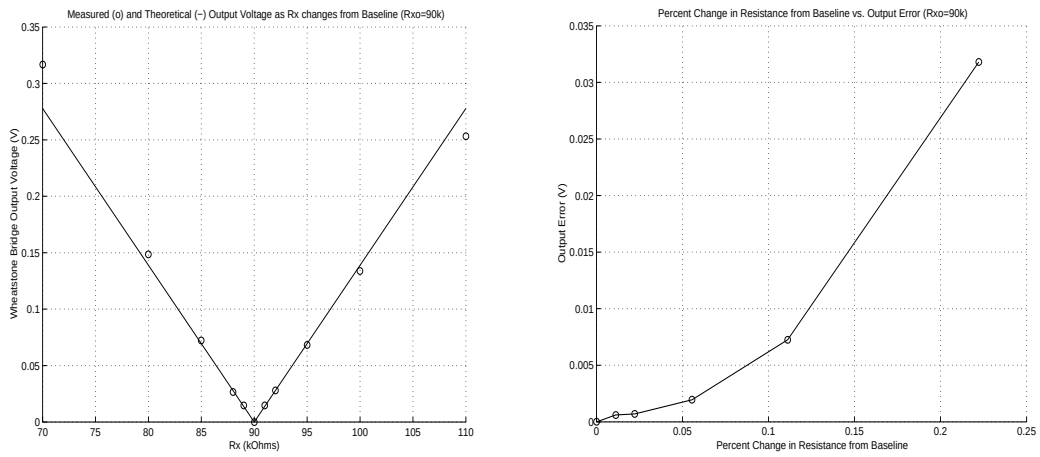

(a) (b)

FIGURE 3-5. Variable-Resistor Auto-Zeroing Baseline Compensator Error

as the resistance changes from the baseline value, the absolute error in the circuit grows exponentially due to loading effects thus vastly limiting the resolution to which analytes can be measured.

SECTION 3.4 DISCRETE VARIABLE-CURRENT AUTO-ZEROING BASELINE COMPENSATOR

An improvement on the variable-resistor auto-zeroing baseline compensation circuit is to use a variable current source instead of a variable resistor. In order to achieve this auto-calibration, a feedback loop is used (Figure 3-6). Using this scheme a user would simply insert a sensor into the circuit and reset it. The level of current necessary to achieve the initial baseline voltage is then automatically applied. Resetting can also be subsequently applied to account for drift. The circuit works as follows. The 8-bit Counter is reset and begins to count up in binary. As the Counter counts a voltage ramp is produced at the Digital to Analog Converter (DAC) output. The output stage converts this voltage ramp to a current ramp going into the sensor. The current ramp going into the chemical sensor causes the voltage across the sensor to increase (for all three sensor types described here). Once the voltage across the sensor reaches a preset threshold value, the comparator shuts off the counter thereby freezing the amount of current going into the sensor. Therefore regardless of initial sensor state, the initial voltage across the sensor is predetermined by the threshold, and changes around this value as chemicals are applied. The counter is then disabled to prevent subsequent changes in the sensor from being unintentionally compensated.

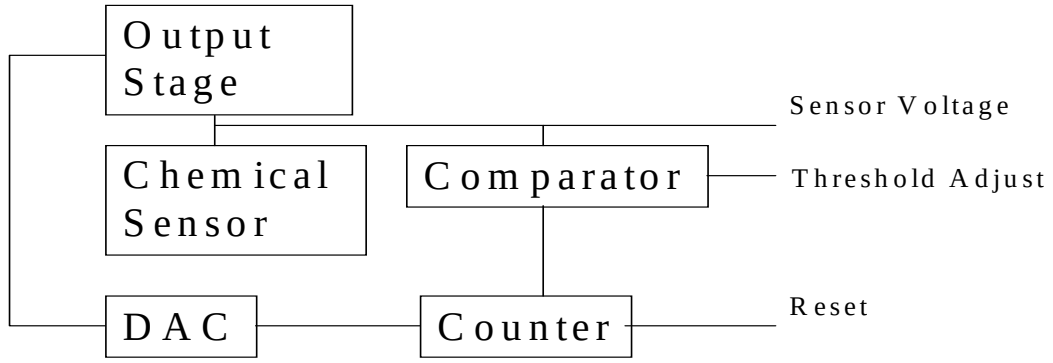

FIGURE 3-6. Compensation Feedback Loop

The compensation feedback loop acts as a variable current source to bias the chemical sensor with the correct amount of current so that the initial sensor voltage was equal to the threshold voltage. The circuit can also be reset and the sensor recompensated to account for drift.

All components of this compensation circuit are straight-forward except for perhaps the output stage. The circuit for the output stage is shown in Figure 3-7. Figure 3-8 demonstrates the entire compensation process. The circuit is a modified instrumentation amplifier acting as a voltage-con-

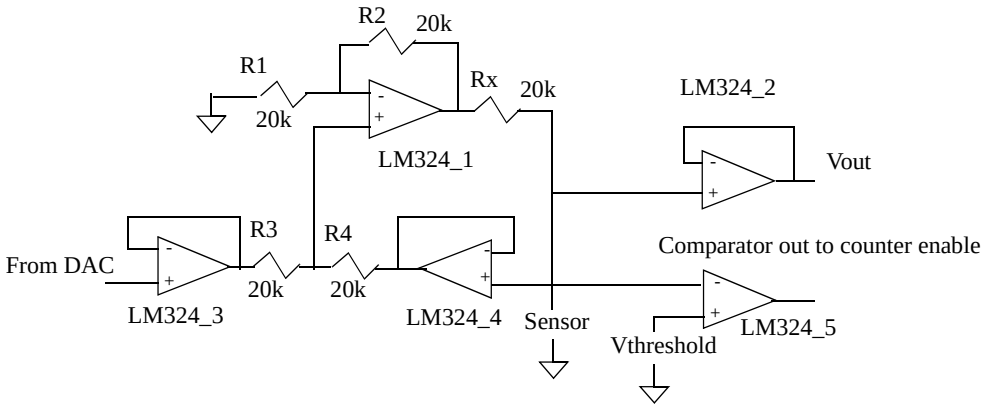

FIGURE 3-7. Output Stage Schematic

The output stage acts as a voltage-controlled current source to bias the chemical sensor at a current that forces the baseline sensor voltage to a predetermined threshold.

trolled current source. Op-amp LM324_4 is bootstrapped to require that the voltage across R_x be equal to the applied voltage from the DAC. Ideally no charge flows into an op-amp input so the voltage across R_x will directly produce a current which was injected entirely into the sensor, producing the sensor output voltage. Therefore,

$$V_{Sensor} = \frac{R_{Sensor} V_{DAC}}{R_x} \qquad \textbf{(Eq 3.3)}$$

$$V_{Sensor} = V_t + \sqrt{\frac{2 V_{DAC} R_x}{k'(W/L)}} \qquad \textbf{(Eq 3.4)}$$

for the chemiresistor and ChemFET respectively. Resistors of size 20kΩ are used in the output stage because their resistance is large enough to limit power consumption, but not so large that their impedances begins to produce significant non-idealities in the op-amps.

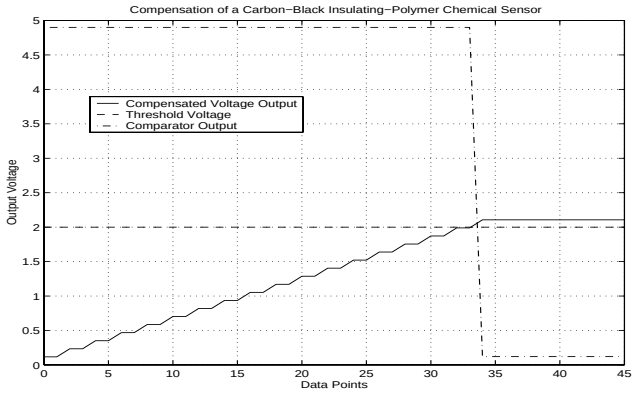

FIGURE 3-8. Composite-Film Polymer Chemiresistor During Compensation

R_x is set to $5k\Omega$, thereby causing I_{set} to go from 0 to 1mA in 3.9μ A steps. The initial resistance of the composite-film polymer chemiresistor is $30k\Omega$. When the sensor voltage output exceeds the threshold voltage of 2V at 2.106V, the comparator changes states, shutting off the current ramp. A more precise compensation could be obtained by using a larger value of R_x, but this action would also limit the range of baseline resistances that could be compensated as demonstrated in equation 3.5.

For the case of chemiresistors, the following formulas are useful in determining what value of R_x to use relative to the expected range of resistances of the chemiresistors (R_{min} to R_{max}). The smaller the range the more accurate the compensation.

$$R_{min} = 0.4R_x \quad \textbf{(Eq 3.5)}$$

$$R_{max} = 20R_x \quad \textbf{(Eq 3.6)}$$

The variable-current discrete auto-zeroing compensation circuit consists of four separate printed circuit boards. Two of the circuit boards contain the auto-zeroing baseline compensation circuits for six sensors and one of the boards contains the sensors. The final board contains digital processing electronics, power inputs, and an optional interface to a data acquisition system made to be used with Lab View.

Empirical results have been collected by placing the compensation circuit and chemical sensors in an enclosed chamber approximately 1 meter in length on each side. The types of sensors used include two types of composite-film polymer sensors (provided by Nathan Lewis at CalTech) and

three types of tin-oxide sensors (purchased from Figaro Engineering). A small container is placed into the test chamber containing the analyte of choice. The container is separated from the chamber by a solenoid valve. Before any analyte is applied to the chamber, the chamber is purged using compressed air. All sensors are allowed to stabilize prior to introduction of an analyte. The solenoid valves are opened for 30 minutes to allow the analyte to diffuse into the chamber, then closed to allow the sensors to return to their baseline values. Typical results for compensated responses for tin-oxide sensors are shown in Figure 3-9 and Figure 3-10. Figure 3-9 demonstrates the limiting of sensor dynamic range, as the three different types of tin-oxide sensors all start at the chosen threshold voltage of 2V to within 3%. Likewise Figure 3-10 demonstrates that compensation does not distort sensor response, but rather the sensor response is simply scaled so that all baseline voltages are identical across the different sensors.

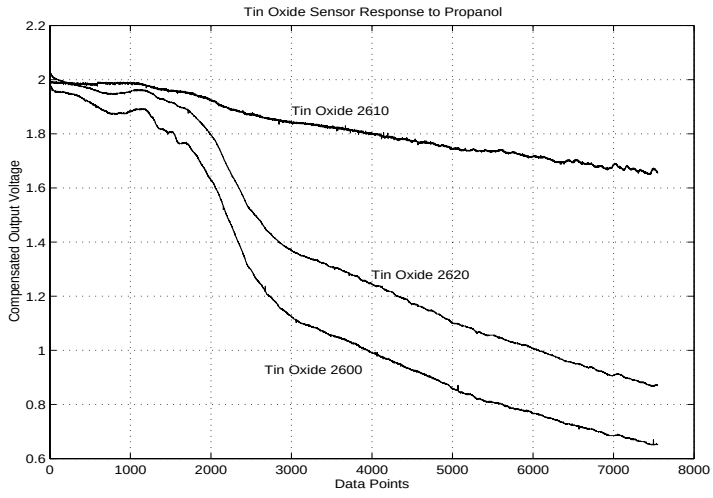

FIGURE 3-9. Response of Tin-Oxide Sensors to Propanol

As the analyte vapor diffused in the testing chamber, the sensor voltage began to decrease. The three types of tin-oxide sensors have been optimized to detect different types of gases and therefore they respond at different rates.

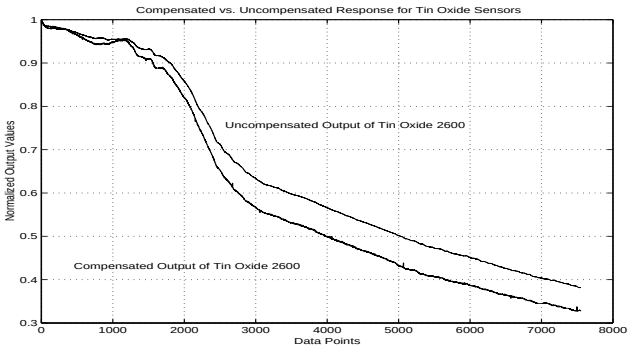

FIGURE 3-10. Normalized Compensated and Uncompensated Response of Tin Oxide Sensors

The above curves are normalized by setting the maximum value in each to 1. Because this compensation scheme does not change the shape of the response, only the scaling, the compensated and uncompensated curves should be nearly identical. The mean squared error between the two curves is 0.0548. The slight discrepancy was due to random fluctuations in gas delivery between sensors as the two sensors were seperated by a distance of several inches and the detection of analyte diffusion into the chamber has been observed to be highly depenent on sensor position within the chamber.

In Table 3-2, measurements were taken of the initial baseline voltage of composite polymer sensors after they have been compensated. The value for R_x used for these measurements is $20\text{k}\Omega$. Ideally the compensated voltage should equal the threshold voltage of 2V. In general, as baseline resistance increases and becomes much greater than R_x, the compensation accuracy decreases. Although the current ramps up in constant intervals, the size of the voltage steps at the sensor output (as determined by Ohm's law) is larger for greater baseline resistances..

Table 3-2 - Measured vs. Ideal Baseline Compensated Sensor Outputs

Baseline Resistance	Compensated Voltage	Threshold Voltage	Percent Difference
$20\text{k}\Omega$	2.016V	2V	0.8%
$50\text{k}\Omega$	2.012V	2V	0.6%
$70\text{k}\Omega$	2.060V	2V	3.0%
$110\text{k}\Omega$	2.051V	2V	2.55%
$200\text{k}\Omega$	2.153V	2V	7.65%

As shown in Figure 3-11, a sensor can be periodically recompensated to account for drift in order to maintain a near constant baseline output. Drift rates noted in our experiments and in experiments done by other labs have typically shown drift to be limited to about 5% per month, unless the sensor becomes poisoned in which case drift can be much higher to the point that the sensor lacks sensitivity and must then be discarded. Under normal circumstances, drift has been shown to not significantly affect sensor sensitivity and when compensated, drift does not effect sensor accuracy [9]. The drift compensation performed in Figure 3-11 demonstrates the value of drift compensation in reducing dynamic range. Drift can be viewed as low-frequency noise, a distortion in the sensor signal that changes very slowly relative to the actual changes that represent analyte concentrations. Drift compensation here effectively acted as an additional type of noise filter that removes the low-frequency noise, thus reducing the dynamic range in this typical case by over 10 mV. 10 mV can represent a large change in sensor state when the sensor is responding to an analyte. Without this drift compensation, drift limits the resolution of the sensor output voltage to 10 mV, thus decreasing accuracy even though baseline compensation reduced the dynamic range as a whole. Also, if the sensor had been allowed to continue drifting, dynamic range can continue to

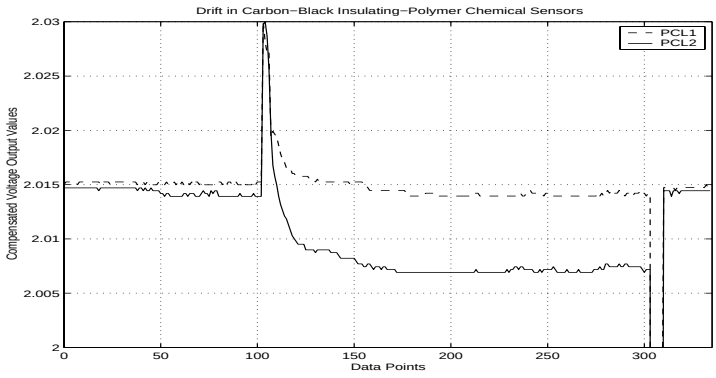

FIGURE 3-11. Drift Compensation in a Composite-Film Polymer Chemiresistors

After compensation, the sensor voltage is approximately 2.015 V. Air saturated with propanol is exposed to the sensors for under a second. The sensors exhibit an increase in resistance due to the analyte and then a decrease in resistance as they returned to a new baseline value. At approximately data point 300, the compensation circuit is reset to establish a new baseline voltage for the sensors, at which time they both return to approximately 2.015V.

increase as baseline values of different sensors diverge. Drift compensation is therefore shown to be a powerful tool in increasing the accuracy of the acquired signal.

SECTION 3.5 INTEGRATED VARIABLE-CURRENT AUTO-ZEROING BASELINE COMPENSATOR

The final version of the auto-zeroing baseline compensator is an integrated one. Integrating the auto-zeroing baseline compensator offers many potential advantages. Circuits can be better optimized to perform compensation because the design takes place at the transistor level rather than at the chip level. Likewise, optimized transistor-based circuits replace resistors present in the discrete design, drastically reducing power requirements. Other advantages of the integrated design over the discrete circuit include size (a factor of 1310 in reduced volume) and cost (a factor of over 40 in reduced cost per compensated sensor).

A block diagram of the integrated auto-zeroing baseline compensation scheme is shown in Figure 3-12. Compensation begins when the system is reset, setting the counter output to zero. The first stage is then externally enabled by bringing both the write-select line on Memory 1 and the Counter enable high. These actions cause Digital to Analog Converter (DAC) 1 to receive four-bit

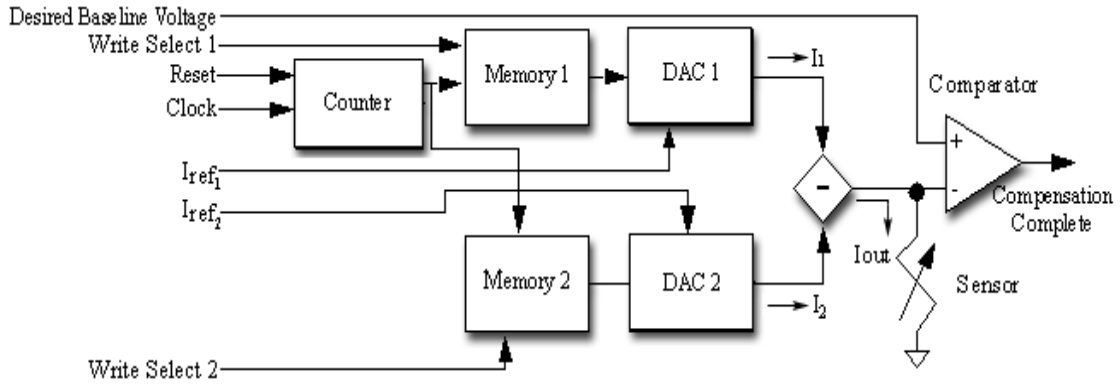

FIGURE 3-12. Block Diagram of Integrated Compensation Scheme

The integrated version of the auto-zeroing baseline compensator incorporates two stages in order to provide accurate compensation while still saving valuable real-estate on the chip die.

binary inputs that are counting up. DAC 1 converted this digital nibble to an analog current. The range of the current is set by an external reference, I_{ref1}, in order to provide flexibility in compensating a wide range of initial sensor states. During compensation, the current injected into the sen-

sor will generate a voltage larger than the desired baseline voltage causing the output of the comparator to go from high to low. The write-select line on Memory 1 is then set low, the Counter reset, and the Memory 2 line set high, thereby enabling stage 2 to begin. Figure 3-13 shows the circuit output as this compensation proceeds.

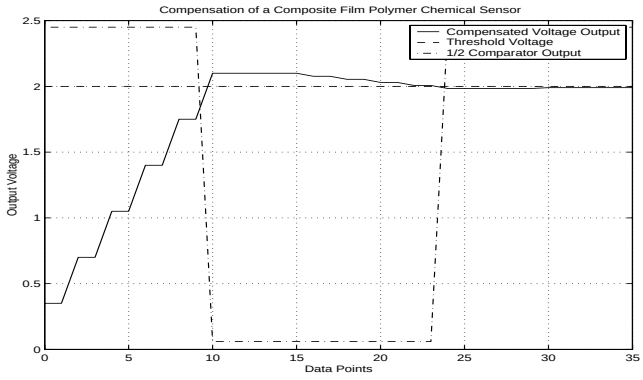

FIGURE 3-13. Integrated Circuit Compensation Process

Rough compensation runs from data point 0 to 10. Fine compensation is performed from data point 15 to 25. Zero average error compensation occurrs at data point 29. The comparator changes states to reflect the compensation stage.

Although external pins provide nearly infinite resolution in setting the bias currents, one possible scheme for setting the bias current of stage 2 follows. In stage 2, the second DAC is biased at a current that was approximately 1/15th that of the first stage. The current from the second DAC is subtracted from that of the first DAC, thereby decreasing the output voltage (by a fraction of the step size in stage 1) as the counter counts up until the comparator again changed states. A final optional step involves switching the final reference current for the second DAC from 1/15th to 1/16th that of the first stage in order to produce a zero average quantization error from baseline. The actual error may be non-zero, however over an array of homogenous sensors, the error will average out to zero as explained in Section 3.9. Subsequent experiments do not incorporate this final step so as to focus on compensation of individual sensors. The DAC is divided into two 4-bit stages to avoid using the large amount of real estate on a single 8-bit DAC and an 8-bit counter. The following equations govern the final baseline voltage:

$$V_b = I_{ref}R_s\left(n_1 - \frac{n_2}{16}\right) \quad \textbf{(Eq 3.7)}$$

$$n_1 = \left\lceil \frac{V_{db}}{I_{ref}R_s} \right\rceil \quad \textbf{(Eq 3.8)}$$

$$n_2 = \left\lceil \frac{15(I_{ref}n_1R_s - V_{db})}{I_{ref}R_s} \right\rceil \quad \textbf{(Eq 3.9)}$$

V_b is the actual compensated baseline voltage; I_{ref} is the reference current for DAC 1; R_s is the sensor resistance; and V_{db} is the desired baseline voltage. Average error across homogenous sensor arrays should be equal to zero to ensure uniformity in consideration of sensor signals in subsequent signal processing. Schematics of key circuit components to the baseline compensator are shown in Figure 3-14. All current mirrors are cascode current mirrors for high output impedance. Refer to Figure 3-12 for signal explanation in the context of the system block diagram.

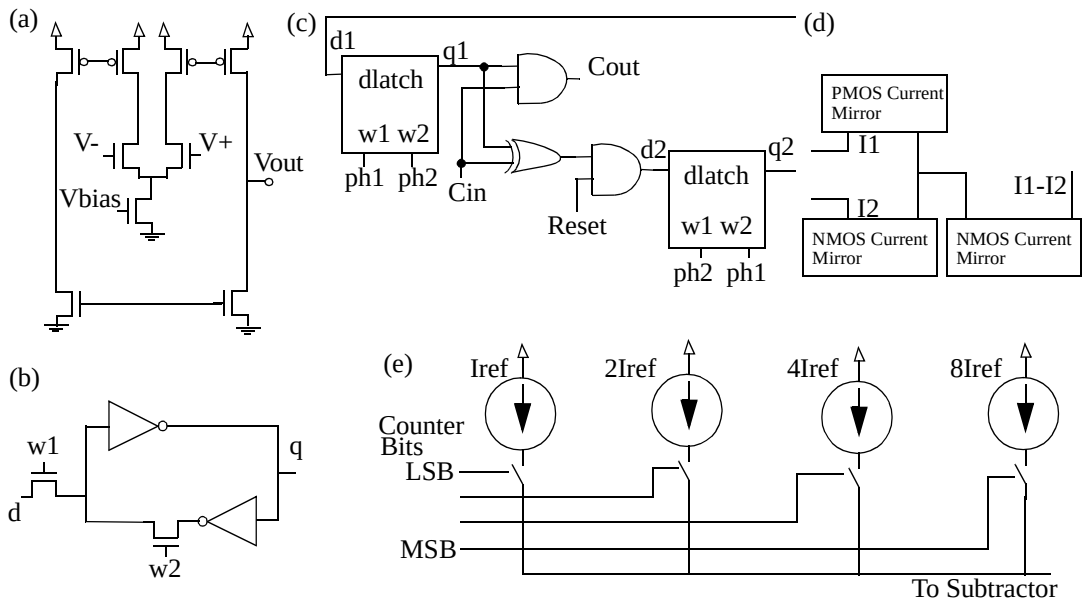

FIGURE 3-14. Schematic of Portions of the Integrated Compensation Circuit.

(a) Schematic of comparator (b) Schematic of dlatch (c) schematic of one-bit of a counter (d) Schematic of current subtractor (e) Schematic of DAC. Note that all current mirrors are cascode current mirrors for high output impedance to minize the effects of loading by the sensor.

The compensation circuit has been fabricated using an AMI 1.5μm n-well process through MOSIS. The available die size is 2.2mm by 2.2mm. Currently compensation circuits for four sen-

sors occupy the die, although expansion for more sensors using the current design is also possible in the future. As described in Section 3.4, the general scheme of compensation employed in the integrated circuit is largely the same as that used in the discrete circuit. The integrated compensation scheme also uses a variable current source, meaning that the sensor response is not distorted. In the case of chemiresistors, sensor resistance is simply multiplied by a constant scaling factor, while in the case of ChemFETs a constant scaling factor is added to the threshold voltage to produce the auto-zeroed baseline voltage. The scaling factor is the determined by the level of current output produced by the current source after compensation has occured.

Experiments have been performed to verify the integrity of the circuit in terms of not distorting the sensor signal. In the case of chemiresistors, Figure 3-15 demonstrates the results of compensating a known resistor of known value, and then subsequently changing the resistor value. Once compensation is performed, the current source should emit a constant current, and so as the resistance changes, the output voltage should change linearly according to Ohm's law. Analysis of Figure 3-15 reveals that as expected Ohm's law was followed. The error produced by deviations from Ohm's law are less than 0.6%, thereby indicating that to a high degree of precision Ohm's law can be assumed to the operating mechanism relating sensor resistance to output voltage. This adher-

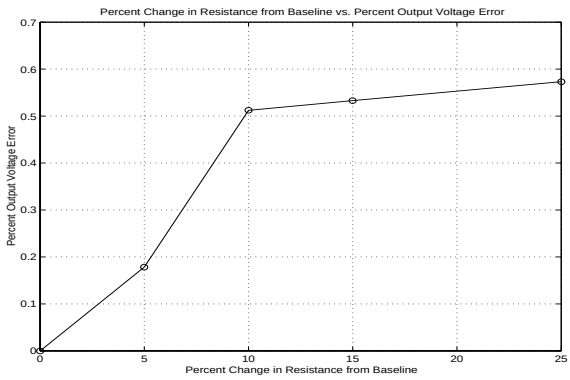

FIGURE 3-15. Current Source Test

Varying the load resistance by 25% produced an average output voltage error of 0.57%. Varying the load resistance by 10% as is more typical for sensor responses, produced an average output voltage error of 0.51%. The baseline resistance used in this experiment is $50k\Omega$.

ence to Ohm's law demonstrates the integrity of the integrated circuit's current source to remain constant under a varying load.

To demonstrate the value of using a two-stage DAC in the integrated circuit, a 100kΩ resistor of constant value is placed in the circuit while the threshold voltage to which the resistor is to be compensated to was varied from 1 to 3 V. Using a single stage, the error between the desired baseline voltage and the measured baseline voltage averages 10% with a range of 5.5% to 16.7%. Using both stages, the error is reduced to under 0.5% with a range of 0.4% to 0.7%.

Two drift tests have been performed on the integrated circuit to demonstrate that the constant current output would not drift over time and to verify that a sensor which had drifted from its baseline value, not in response to an analyte could be recompensated. In the first case, a fixed value resistor is attached to the circuit output and compensated to a threshold voltage of 2V. Due to quantization error, the actual compensated voltage is 2.013V. Measurements taken at as much as 24 hours later show that the output voltage had remained within 2mV of the original compensated value.

As mentioned the second part of the drift test verifies the feasibility of drifting sensor recompensation. The typical result shown in Figure 3-16 demonstrates that indeed drift compensation is possible in the integrated circuit. The recompensated value is only 0.03% different from the original baseline voltage.

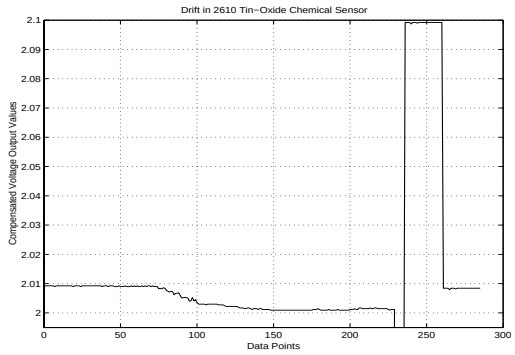

FIGURE 3-16. Drift and Recompensation in a 2610 Tin-Oxide Chemical Sensor

Figure 3-17 shows the measured error in compensating chemiresistors of varying baseline resistances to a baseline voltage of 2V for both one and two stages. The bias current for the second stage is set at 1/16 that of the first stage. In this case, the circuit is calibrated to be able to compensate a minimum resistance of $25k\Omega$, typical of tin-oxide chemiresistors. As the baseline resistance deviates from this value, the baseline compensation error increases. Accurate compensation is possible for a wide range of baseline resistance, but accuracy increases as the possible resistance range is better understood.

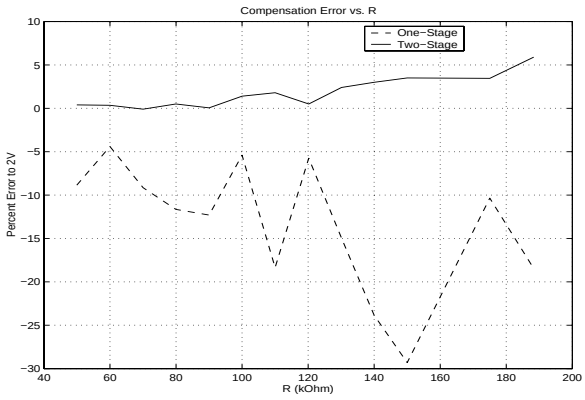

FIGURE 3-17. Compensation Error vs. Baseline Resistance

In an experiment designed to demonstrate the improvement in analyte detection resolution provided by baseline compensation, two composite film polymer chemiresistors, one compensated and one uncompensated, are used to determine which of the sensors first responds to an analyte. The analyte is placed in an open jar two feet from the sensors. One sensor is paired with a $50k\Omega$ divider resistor for readout. The other sensor is placed in the compensation circuit. Using a standard 12-bit data acquisition card, the minimum detectable voltage is 1.2mV. The compensated circuit detects the analyte after 20 seconds by responding by at least the minimally detectable voltage, while the non-compensated circuit took over twice as long. The compensated circuit has demonstrated over twice the resolution for concentration detection in this experiment.

SECTION 3.6 NOISE FILTERING

Noise filtering can play an important role in chemical sensor signal extraction, especially in combination with auto-zeroing baseline compensation. Figure 3-18 demonstrates the value of noise

reduction. Typically the ChemFET output voltage changes by a maximum of a couple hundred millivolts in high concentrations of analytes. The unfiltered signal here covers a range of over 15 mV, a significant percentage of the maximum possible dynamic range of the ChemFET. The modes of noise reduction used here improves the signal to noise ratio by nearly 25 dB. Baseline compensation first reduces the sensor dynamic range to a constant range for all sensors, and noise reduction then maximizes signal extraction from within this constant range.

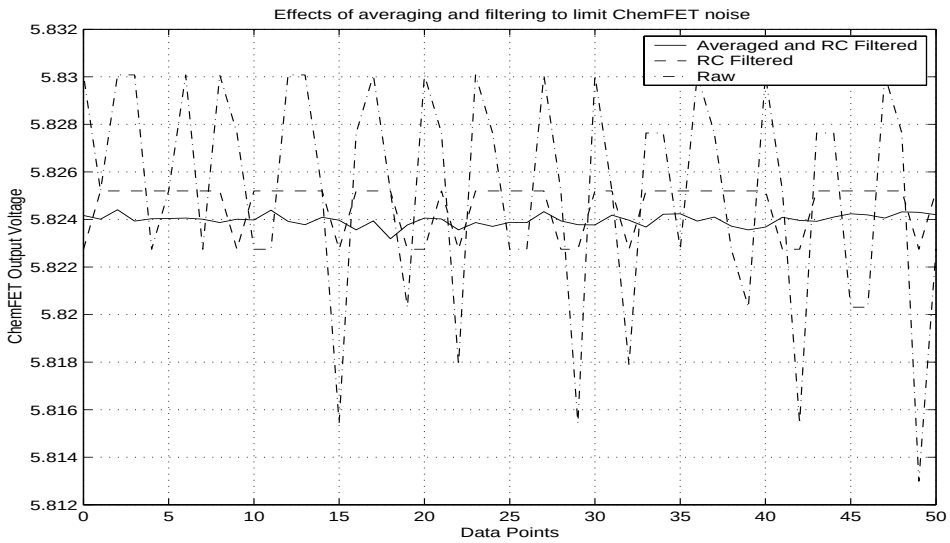

FIGURE 3-18. ChemFET Noise

Noise present in ChemFET at standard temperature and pressure with no analyte present is shown. Before filtering, significant noise is present, with a signal to noise ratio of 61.7 dB. After hardware filtering, the signal to noise ratio is improved to 73.7 dB. The hardware filter is a simple first order RC-filter with a cutoff frequency of 8 Hz. Finally, after both hardware and software noise reduction, the signal to noise ratio is further improved to 85.2 dB. The noise is caused by a combination of flicker noise, thermal noise, data acquisition noise and other sources.

SECTION 3.7 COMPARISON OF DISCRETE AND INTEGRATED COMPENSATOR CIRCUITS

Some limitations exist for the discrete circuit design. For example, the resolution to which the sensor is baseline compensated is limited by number of possible states (number of bits on the counter) and by the range of the current ramp (set by R_x) as shown in Table 3-2. For an 8-bit counter, 256

possible states are evenly divided within the current ramp range. Increasing the range of the current ramp enables the compensation of a wider range of initial sensor states, but at lower resolution. In the case of the discrete circuit, baseline compensation is also further diminished by non-idealities in the op-amps used throughout the circuit, especially in the case of the composite-film polymer chemiresistors which typically have a high initial impedance relative to the other sensor types. Initial output impedances of the composite-film polymer chemiresistors can easily be on the order of several hundred $k\Omega$. Another issue with the op-amp is the finite input bias current. The combined bias current that leaks into the various op-amps at the sensor node should be approximately $1\mu A$ and is variable with temperature. In the case of the composite-film polymer chemiresistors, the bias current passed through the sensor by the compensation circuit is generally below $100\mu A$. Because the leakage current is a significant fraction of the compensation current for this sensor type, significant degradation in the predicted circuit response is possible. In addition, the present layout of the circuit requiring the sensor to be connected from various op-amp inputs to ground may also degrade the input impedance of the op-amps to which it is connected, further increasing bias currents and limiting the ability of the voltage followers to correctly follow their input voltages. However, Table 3-2 indicates that even taking into account the various non-idealities of the op-amps, the circuit still performed compensation to a high degree of accuracy.

The integrated circuit allows many design simplifications to take place that further optimize the circuit for its intended purpose beyond what is possible with discrete chips. Many of the problems associated with the op-amp non-idealities disappear as a different method is used to generate the current ramp not involving op-amps. Compensation errors in the integrated version should then be less than that for the discrete circuit. Table 3-3 demonstrates the measured results. As expected, the average percent compensation error for the integrated circuit is nearly twice as small as that for the discrete circuit (1.69% for the integrated circuit compared to 2.92% for the discrete circuit).

Table 3-3 - Discrete vs. Integrated Compensated Sensor Outputs

Baseline Resistance	Discrete Compensated Voltage	Integrated Compensated Voltage	Ideal Compensated Voltage	Percent Difference for Discrete	Percent Difference for Integrated
$20k\Omega$	2.016	1.995V	2V	0.8%	0.25%
$50k\Omega$	2.012	1.992V	2V	0.6%	0.4%

Table 3-3 - Discrete vs. Integrated Compensated Sensor Outputs

Baseline Resistance	Discrete Compensated Voltage	Integrated Compensated Voltage	Ideal Compensated Voltage	Percent Difference for Discrete	Percent Difference for Integrated
70kΩ	2.060	2.002V	2V	3.0%	0.1%
110kΩ	2.051	1.964V	2V	2.55%	1.8%
200kΩ	2.153	1.882V	2V	7.65%	5.9%

Because the integrated circuit produces a smaller compensation error, the resolution to which analytes can be measured is improved. For example, when including the effects of quantization error, and using a 12-bit A/D converter with typical composite-film polymer chemiresistors, the minimum detectable change in concentration for cyclohexane is 0.254 ppm for the integrated circuit, while the for the discrete circuit, this minimum detectable change in analyte increases to 0.257 ppm, a slight but appreciable decrease in resolution which in cases involving hazardous chemicals could be critical.

Besides compensation performance, the integrated version of this circuit offers many other advantages over the discrete version. Current draw (and therefore power consumption) drops tremendously from approximately 100mA per sensor in the discrete circuit to milliamp levels in the integrated circuit. Integrated circuits are also smaller than discrete circuits thereby leading to more portability. In this case as discussed in Section 3.5, the discrete circuit takes up a volume of approximately 1310 cm^3 while the equivalent integrated circuit occupies approximately 1 cm^3. In addition, an integrated circuit reduces cost. The discrete version costs approximately $40 per sensor compensated even when mass-production is taken into account, while an integrated chip costs only a few dollars and houses compensation capabilities for multiple sensors. Finally, since all sensors chosen for this research effort are silicon-compatible, in the long-term, they can be fully integrated with processing circuits, further reducing power, space, and cost at the system level.

SECTION 3.8 AUTO-ZEROING BASELINE COMPENSATOR CAPABILITIES

Using the compensation loop discussed previously from Figure 3-12, the input-output equation for the composite-film polymer chemiresistor changes as shown:

$$Uncompensated \Rightarrow \frac{\Delta R}{R_o} = k[C] \quad and \quad \Delta R = R - R_o \Rightarrow R = R_o + R_o k[C] \qquad \textbf{(Eq 3.10)}$$

$$Compensated \Rightarrow V_o = I_{Set} R = I_{Set} R_o \left(1 + \frac{\Delta R}{R_o}\right) = I_{Set} R_o (1 + k[C]) = V_b (1 + k[C]) \qquad \textbf{(Eq 3.11)}$$

The compensated curve produces curves that have a constant sensitivity of $V_b k$ which means that slope of the compensated curve is unaffected by the baseline resistance. The reduction in input dynamic range is demonstrated in Figure 3-19. Before compensation, the baseline resistance of the

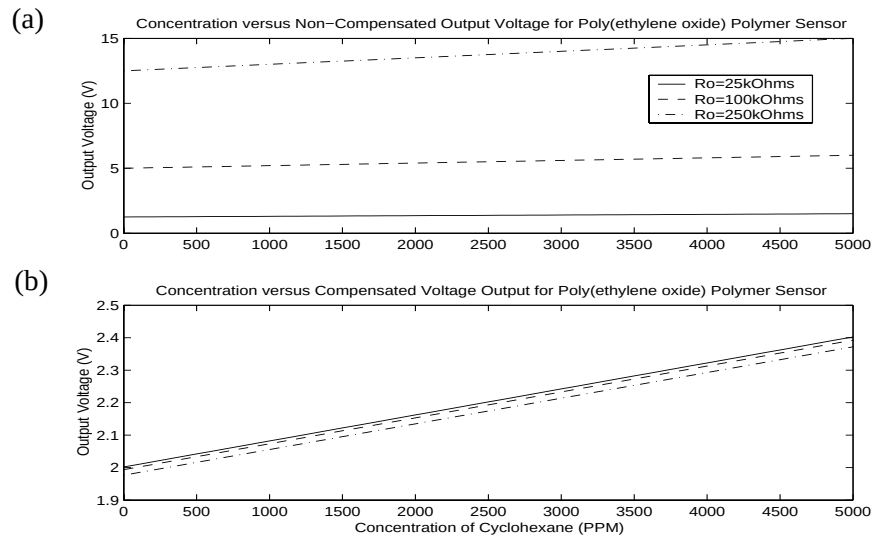

FIGURE 3-19. Simulation of Compensated and Uncompensated Sensor Response

(a) demonstrates the wide dynamic range needed to accommodate uncompensated sensor responses over varying baseline voltages. (b) demonstrates the dramatic decrease in compensated dynamic range. The values obtained in (b) for different baseline resistances are not exactly the same due to quantization error.

poly(ethylene oxide) chemiresistors varies from 25kΩ to 300kΩ, as is typical due to manufacturing variation. The sensor resistance is extracted as a voltage by injecting a constant current into the resistor and measuring the resulting voltage across the resistor. For example, using a constant current of 50μA and assuming that the sensor resistance could change by as much as 20%, the range of output voltages possible is 1.25 V to 18 V. With a 12-bit analog-to-digital converter (ADC) the minimum detectable change in either sensor is 81.8Ω (0.327% to 0.027%). When using compen-

sation, the minimum detectable change is 2.4Ω to 29.3Ω (0.010%), produced from a voltage range of 2 to 2.4V. Without compensation, if it is desired to obtain similar resolution levels as that obtained with compensation, an ADC with more than 17-bits would have to be used, greatly increasing power, cost, and space requirements. Compensation provides up to a factor of 34 improvement in response (e.g. concentration) resolution for the same sensors and electronic processing. Likewise, the minimum detectable change in concentration of cyclohexane for the non-compensated circuit is 16.4 ppm, while for any of the compensated sensors, the minimum detectable concentration change is 0.5 ppm. The compensation circuit has greatly enhanced the detecting capability of these chemical sensors by improving resolution and detection limit.

In a good sensor interface circuit design, it is the sensor noise that limits the minimum detectable value and not the circuit into which the sensor is placed. As previously calculated, the thermal noise associated with a composite-film polymer chemiresistor of 100kΩ should be about 0.129 mV. With a 12-bit A/D converter, the minimum detectable voltage change is 0.098 mV. Thus, the sensor noise limits the minimum detectable value, further verifying the validity of the design. The previously discussed RC noise filter also aids in further reducing the noise from that expected from calculations, ensuring that this minimum detectable signal is representative of the sensor response.

Similar analysis can be performed for the other two sensor types as well. For the tin-oxide sensors the compensated input-output equation reduces to:

$$V_o = V_b\left(\frac{I_{set}}{I_{set} + V_b k[C]^r}\right) \qquad \textbf{(Eq 3.12)}$$

It can be seen here that at zero concentration of analyte, the output voltage becomes the baseline voltage and that as the analyte concentration increases, the output voltage decreases towards zero. As it was with the composite-film polymer sensor, the relationship between sensor resistance and output voltage is preserved, but is scaled by a constant factor.

In the case of ChemFETs, the output dynamic range, and therefore the concentration detection resolution is also reduced as follows. By examining the governing transduction mechanism Equation 2.7, adjusting the bias current has the effect of adjusting the y-intercept of the response in such a way that all chemFETs respond in a similar voltage range. If the bias voltages that act to set the

reference currents are tabulated for known sensor technologies, it becomes possible to use this compensation circuit in a plug and play manner to improve system concentration resolution and linearity.

After compensation for the chemFET sensors, the compensated output voltage is:

$$V_o = x_o \ln(a[C]) + x_2 \qquad \textbf{(Eq 3.13)}$$

The new constant *x2* incorporates *x1* and the term containing the drain current from Equation 2.7 as this has now been fixed as a constant. One boundary condition that exists is that as the concentration approaches zero, the output voltage approaches the baseline voltage set by the compensator. As with the chemiresistors, comparison of the modified input-output equation shows that the nature of the relationship is the same with the addition of scaling factors. The response is not distorted, and therefore becomes more useful for such applications as transient response analysis.

As sensor baseline states drift over time, typically 3% over the course of a week, sensors need only to be recompensated to return them to the desired baseline output voltage. Because drift does not significantly affect sensor sensitivity, this recompensation effectively eliminates the effects of low-frequency drift. Other post-processing methods incorporated into the principal component analysis can further reduce the effects of drift [28].

Other types of drift occur in response to changes in environmental parameters. For example, as previously mentioned tin-oxide chemiresistors are highly sensitive to humidity in the environment. To overcome this difficulty an on-board humidity sensor can monitor humidity, and indicate when humidity changes by an appreciable amount, at which time sensors should be recompensated so that any subsequent change in sensor state is due to the introduction of analytes and not environmental changes. Further post-processing adjustments can be made digitally. For example, models incorporating information on not only the instantaneous humidity, but how long sensors spend at different humidity levels have been shown to produce more accurate results [29].

SECTION 3.9 IMPACT OF QUANTIZATION NOISE ON SYSTEM PERFORMANCE

An additional type of noise from those discussed in Section 2.4 is quantization noise. In a large homogenous array of sensors, the average output voltage is:

$$V_{av} = V_b(1 + k_a[C]) + \Delta_{av}(1 + k_a[C]) + \delta_{av}V_b + \Delta_{av}\delta_{av} \quad \textbf{(Eq 3.14)}$$

V_{av} is the average output voltage of the array; k_a is the sensor constant of the homogenous array; Δ_{av} is the average of quantization error caused by the DAC; δ_{av} is the average error in actual sensor response from k_a caused by variances in manufacture. Note that this equation assumes that the quantization noise error and sensor error are independent. In the case where, Δ_{av} and δ_{av} are both equal to zero, the equation reduces to the desired form of:

$$V_{av} = V_b(1 + k_a[C]) \quad \textbf{(Eq 3.15)}$$

Figure 3-20 shows the quantization noise error produced in compensating a wide range of baseline resistance values, assuming that the minimum value to be detected is 25kΩ. (a) represents the quantization error for an 8-bit DAC used with baseline resistances ranging from 25kΩ to 300kΩ and V_{db}=2V. The 8-bit error range and mean were 94.6 mV and 2.026 V respectively. (b) represents the quantization error if a two-stage (4-bits per stage) DAC was used, also with V_{db}=2V. The two stage error range and mean were 132.6 mV and 2.001 V respectively.

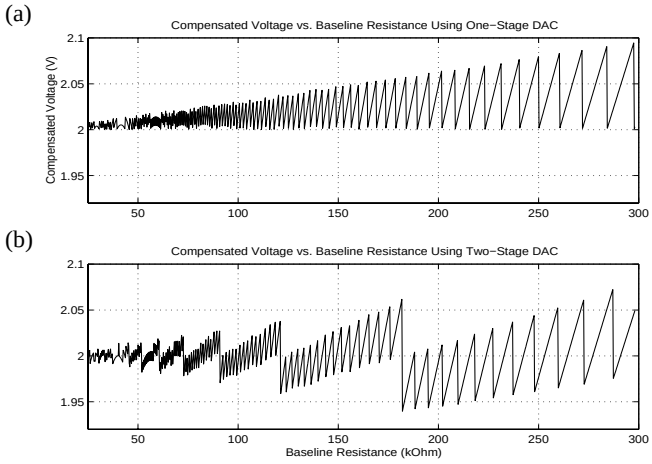

FIGURE 3-20. Quantization Noise of Traditional One-Stage DAC (a) vs. Two-Stage DAC (b)

The compensated equations for tin-oxide and ChemFET chemical sensors, while not as straightforward as that for the composite-film polymer chemiresistor still enable a reduction in the output dynamic range.

SECTION 3.10 HOMOGENOUS SENSOR ARRAYS

Certain issues with accurate chemical sensor signal extraction can be overcome with the use of homogenous sensor arrays. Homogenous arrays consist of sensors of nearly identical parameters such as sensor type, coating, and dimensions which can be safely assumed to have an aggregate normal distribution. As the size of the array increases, the variance of random variations between sensors such as temperature and gas delivery fluctuations changes according to:

$$\sigma_{array} \propto \frac{1}{\sqrt{N}} \qquad \textbf{(Eq 3.16)}$$

N is the number of sensors in the homogenous array. This principal of decreased array variance with increased amounts of homogenous sensors has been demonstrated successfully [30]. While random variations can be overcome by increasing the number of sensors, systematic variations such as drift, fluctuating environmental parameters like humidity, and sensor poisoning cannot be overcome in this way. The compensation abilities of the auto-zeroing baseline compensation circuit provide a solution for reducing the effects of systematic variations.

Occasionally, sensors may become poisoned in a non-recoverable way when the sensor surface becomes saturated with analyte. If sensors are in a homogenous array of the same sensor type, statistical analysis can be performed to eliminate sensors which have potentially become poisoned. Because the sensor signal is redundant there is no negative effect on the discriminating ability of the array as a whole, especially in the case where a poisoned sensor is replaced by a new healthy one. For example, if all sensors in a homogenous array have been baseline compensated to baseline values, simple digital post-processing can look at the signals to see if there are any aberrant sensors which differ from the correct baseline value by more than a specific amount, generally more than two standard deviations from the mean of the remaining sensors. Such sensors can then electronically or physically be removed from the sensor array and replaced with functional sensors.

SECTION 3.11 INTERFERENT COMPENSATION

The purpose of the interferent rejection circuit shown in Figure 3-21 is to enable better discriminate primary analytes in the presence of other chemicals known to interfere with the primary analyte's detection. Often interferents are chemicals in the same family as the primary analyte and thus are more difficult for sensors to discriminate among. This circuit is loosely based on the way mitral cells in specific regions of the olfactory bulb tend to respond to similar chemicals, and also tend to cross-excite and cross-inhibit one another to better detect primary analytes in the presence of interferents [31].

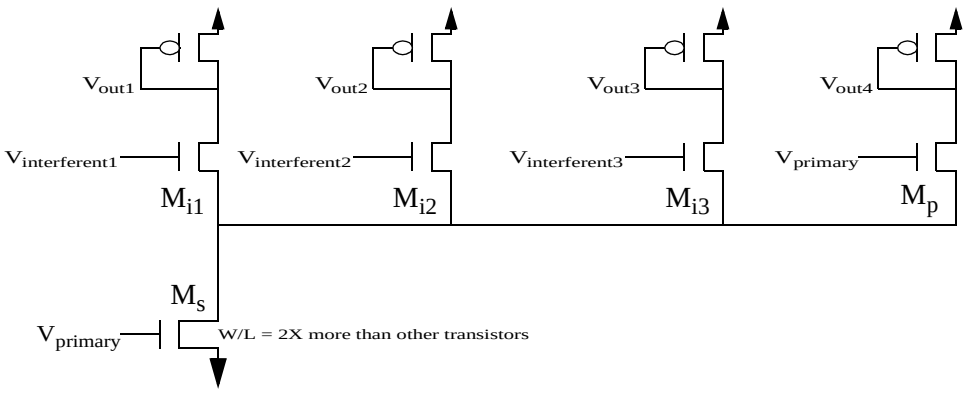

FIGURE 3-21. Biologically-Inspired Interferent Rejection Circuit

In the interferent rejection circuit, M_s acts as a current source modulated by the detection of a primary analyte. This current is further modulated by the outputs of sensors designed to respond well to interferents of the primary analyte. If the analyte causes a response from the sensor designed to detect the primary analyte and the one designed to detect interferent 1, then both V_{out1} and V_{out4} will respond, indicating that an interferent is present and must be taken into account in subsequent processing. Also, M_{i1} will partially turn on, causing some of the current that would have passed through M_p to pass through M_{i1} instead, thus the response at V_{out4} is automatically reduced as it should be because it is responding in part to the interferent. Figure 3-22 demonstrates this reduction as interferents of different levels are applied. No interferent generates 0V across the $V_{interferent}$ inputs. Low interferent generates 2V, while high generates 5V. The primary input signal is set to vary from 3.5 to 4.5 over the span of 10 msec. The current source used is 32µ/1.6µ in size. Figure 3-23 shows the effect of a changing interferent level on the output compared to no interfer-

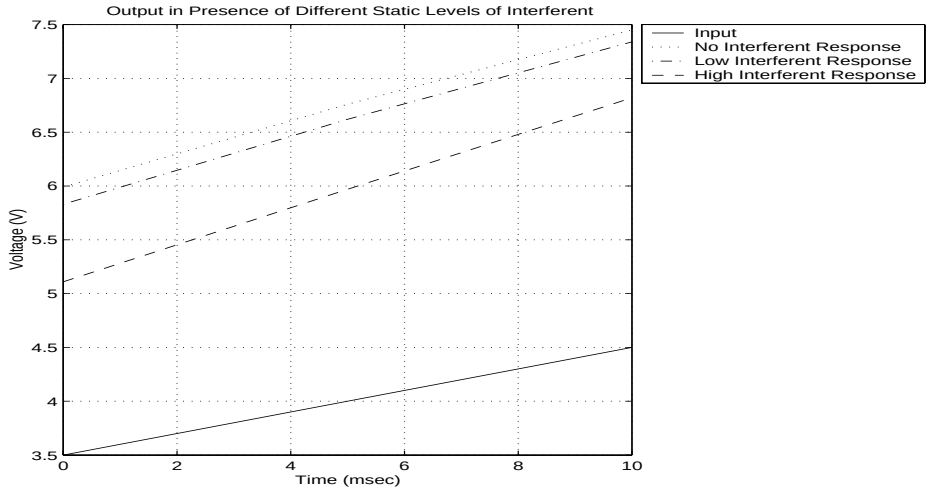

FIGURE 3-22. Output in Presence of Different Static Levels of Interferent

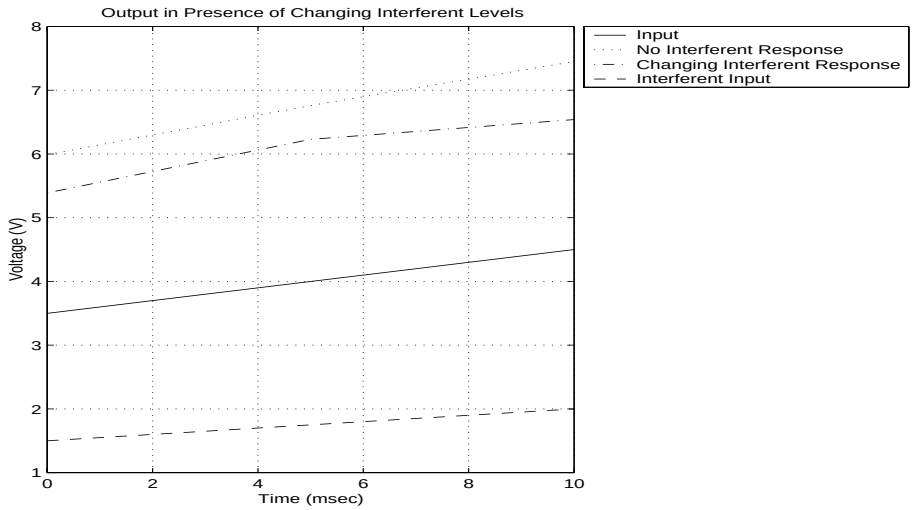

FIGURE 3-23. Output in Presence of Changing Interferent Levels

ent. As expected the level of interferent present increases, the primary output decreases to reflect that a larger portion of the response is due to interferent.

ChemFETs have been manufactured with sensors designed to respond to primary analytes and interferents all on the same chip, making implementation of this sort of circuit highly straightfor-

ward. Due to the compensation circuit being used here, baseline values for different interferents can be set to different values to maximize extraction of the primary analyte signal. The final fabricated circuit uses three different sized current sources. Use of different current sources provides another method getting the outputs in the general desirable range as shown in Figure 3-24. The input in this plot is the primary analyte.

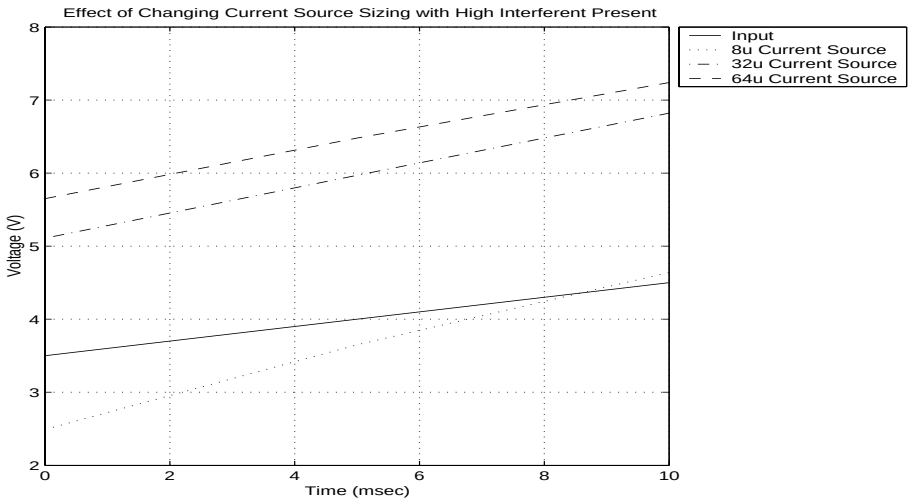

FIGURE 3-24. Effect of Changing Current Source Sizing

The simulation results above demonstrate the ability of the interferent circuit to modulate the response of the circuit in the presence of interferents. Baseline compensation is an enabling factor for this circuit to work properly in the setting of interferent voltages at similar dynamic ranges across different sensor technologies and fabrication variations.

This circuit has been fabricated on the same die as the auto-zeroing baseline compensator using a 1.5µm N-well process through the MOSIS foundry. Experimental results shown in Table 3-4 verify the validity of the simulation results presented above. Average deviation from the expected simulation results is under 3%..

Table 3-4 - Simulated vs. Experimental Interferent Rejection Circuit Results

V_{i1}	V_{i2}	V_{i3}	V_p	Current Source	Simulated Results	Experimental Results	Percent Difference
0V	0V	0V	3.5V	32µ	4.01V	4.12V	2.7%

Table 3-4 - Simulated vs. Experimental Interferent Rejection Circuit Results

V_{i1}	V_{i2}	V_{i3}	V_p	Current Source	Simulated Results	Experimental Results	Percent Difference
0V	0V	0V	4.5V	32µ	2.55V	2.60V	2.0%
2V	2V	2V	3.5V	32µ	4.17V	4.20V	0.7%
2V	2V	2V	4.5V	32µ	2.66V	2.72V	2.3%
5V	5V	5V	3.5V	32µ	4.89V	4.95V	1.2%
5V	5V	5V	4.5V	32µ	3.18V	3.30	3.8%
3V	5V	7V	3.5V	32µ	4.75V	4.92	3.6%
3V	5V	7V	4.5V	32µ	3.09V	3.21	3.9%
5V	5V	5V	3.5V	8µ	7.51V	7.88	4.9%
5V	5V	5V	3.5V	64µ	4.35V	4.55	4.6%

CHAPTER 4 *System Integration and Summary*

This chapter looks at system level applications of chemical sensors using the discrete auto-zeroing baseline compensator. The automated nature of the discrete auto-zeroing baseline compensator as well as its ability to compensate over a wide range and over chemiresistors and ChemFETs make it a good candidate for use in system level applications. Future system applications using the integrated auto-zeroing baseline compensation circuit should further improve results. Intelligent post-processing using principal component analysis in combination with the reduced dynamic range created by compensation creates a visual display of chemical sensor responses that can easily be analyzed using built-in human classification abilities.

This chapter also includes suggested areas of research which could build on the results presented in this research effort. Finally, the main points and results of this effort are concisely summarized for reference purposes.

SECTION 4.1 TRANSIENT RESPONSE CHEMICAL DISCRIMINATION MODULE BACKGROUND

The portable chemical discrimination module combines arrays of homogeneous sensors for reasons discussed in Chapter 3 to improve noise performance and detecting broken sensors with heterogeneous arrays of sensors to discriminate among analytes of interest. Sensors can be modularly added to or removed from the measurement module. Using these sensors, the module supplies the

user with real-time chemical discrimination information that tracks the response vector of the sensor as it proceeds from baseline to its steady-state location in multidimensional sensor space. The module includes slots for homogeneous arrays of sensors, heterogeneous arrays of sensors, plug-and-play signal conditioning modules, and a microcontroller for converting normalized sensor signals for display in two-dimensional principal component space.

At the single sensor level, the signal conditioning circuits are designed to process chemical sensor signals in such a way that similar dynamic range and baseline states are ensured at the output of the sensor signal conditioning, regardless of sensor drift, type or fabrication variation. As discussed in Chapter 3, baseline compensator circuits use a sensor calibration feedback loop to normalize sensor baseline states, so that the response of each sensor begins at the same value. Auto-zeroing baseline compensation ensures that the dynamic range of the sensor output is completely consumed by response to analytes rather than to changes in baseline caused by variations in manufacturing. Removal of the effects of baseline variation reduces the number of bits required for a given concentration resolution, thereby reducing power and cost requirements for the portable module.

SECTION 4.2 INTERCHANGEABLE SENSOR INTERFACE

As previously noted in Chapter 3, the compensation mechanism used here is largely sensor independent. Three factors prevent this compensation technique from complete sensor-independence. These factors are the impact of sensor settling, the range of values of the initial sensor baseline parameters, and the value to which sensors of different types are to be compensated.

R_t governs the time that the compensation circuit is enabled. Disabling prevents compensation from occurring when the sensor is legitimately changing in response to an analyte. The time t, in seconds that the compensation circuit will be enabled based on a monostable timer is:

$$t = 1.1 \cdot 10^{-6} R_t \qquad \textbf{(Eq 4.1)}$$

In general it has been observed and can be explained by sensor manufacturing techniques that ChemFETs take longer to settle during compensation and so will require a longer enabling time than the chemiresistors. In the context of the system block diagram, R_t affects the enable pin on the counter in Figure 3-6.

As previously discussed, the resistor R_x also affects the range of compensatable sensor parameters and is influenced by sensor technology. For example, minimum baseline resistances for tin-oxide sensors tend to be much less than those for composite film polymer sensors and therefore are better optimized by using a smaller value for R_x. R_x is shown in the circuit diagram of Figure 3-7.

The final parameter, V_{th}, sets the voltage to which the sensors are compensated. For the chemiresistors, this voltage is a trade-off between power (high values) and noise (low values). A typical value is 2V. However, in the case of the ChemFET, V_{th} must be large enough to ensure that the ChemFET is in the saturation region of operation to ensure proper functionality. This voltage is fairly large because of current peculiarities of the fabrication process in which the ChemFETs are not annealed after fabrication in order to avoid other complexities that could detrimentally affect sensor properties. A typical value is 5V. V_{th} is shown as $V_{threshold}$ in the circuit diagram of Figure 3-7.

In order to make this module capable of plug and play interchangeability, circuit boards have been fabricated that contain both the sensors of interest as well as control of R_t, R_x and V_{th}. Figure 4-1 shows the compensation process for both the mixed sensor board (a) and the tin-oxide board (b).

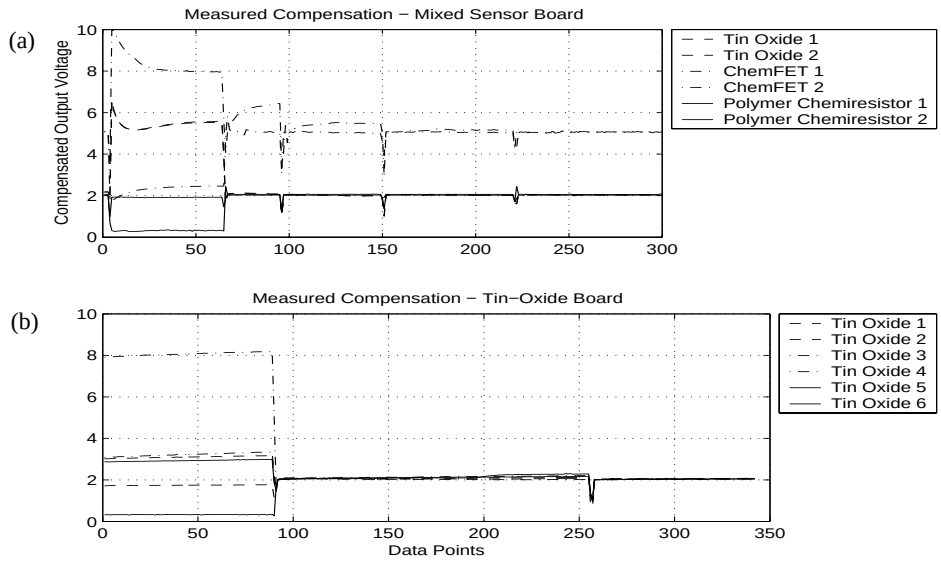

FIGURE 4-1. Measured Compensation of Multiple Sensor Types

The first sensor board consists of six tin-oxide sensors, with two each of three different types. The second board contains two tin-oxide sensors, two composite film polymer sensors, and two chemFETs. Multiple compensations occur in both (a) and (b) due to sensor settling. The module shows no difficulty in compensating for these significantly different combinations of sensors.

SECTION 4.3 OUTLIER REMOVAL

At the homogeneous array level, additional signal processing reduces noise and removes outlying signals corresponding to corrupted sensor outputs. Software on the module has the capability to be programmed with sensor types present in the array currently being used. For specific types of sensors, drift rates are known a priori, and are typically on the order of days. Therefore, if either a signal is more than one standard deviation away from the mean of its sensor type or the sensor drifts by more than 80% over a period of time on the order of days the sensor will classified as an outlier, and its signal will be removed from subsequent processing. If the drift rate is less than 80% the sensor can simply be recompensated to eliminate the effects of drift. Sensor removal occurs if the software detects a sensor signal that is over one standard deviation from the mean of that sensor type. The reduction of dynamic range performed by the compensation circuit is an enabling factor of this feature. Figure 4-2 demonstrates the process of outlier removal. In (a) Sensor 2 and 3 con-

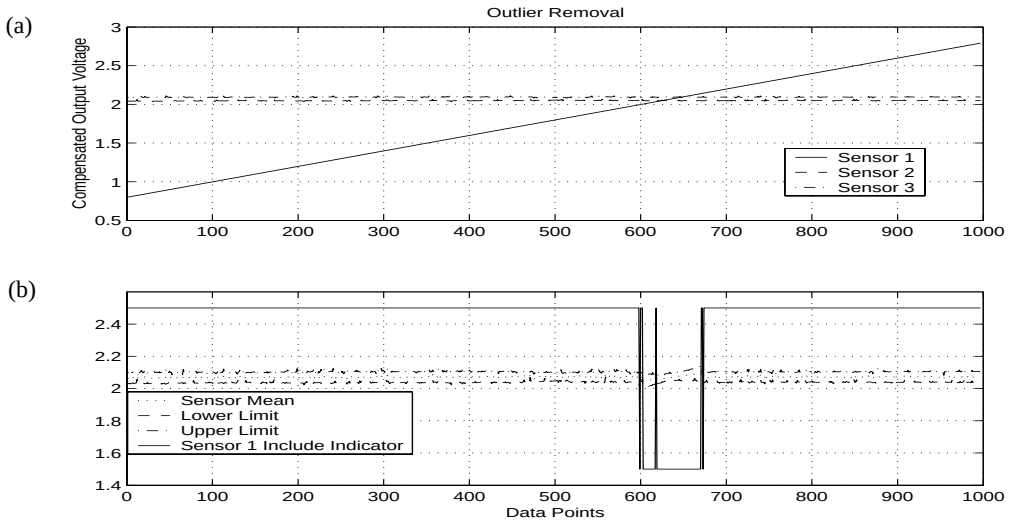

FIGURE 4-2. Outlier Removal

tain real sensor data, while Sensor 1 is a simulated ramp. (b) shows the results of outlier removal on the sensor average as Sensor 1 moves out of the acceptable range defined by one standard deviation from the sensor mean for that type of sensor.

SECTION 4.4 PRINCIPAL COMPONENT ANALYSIS

This research effort uses principal component analysis to discriminate between different types of analytes. Linear feature reduction methods in the past has been found to produce moderately robust results with minimal computational burden while non-linear techniques like artificial neural networks produce a more robust response, but at much greater computational expense [30]. Intelligent pre-processing such as baseline compensation, noise filtering, and outlier removal have the effect of enhancing the discrimination abilities of this module.

Figure 4-3 demonstrates initial results of principal component analysis, used here for analyte classification purposes. Data is taken using three different types of composite film polymer chemiresistors using no compensation, and using the integrated compensation circuit. The sensors are placed in a sealed chamber into which the analyte is allowed to diffuse. Measurements continued until the sensors reach a steady-state response. The figure shows the euclidean distance between the two-dimensional principal component transformed data for responses to Methanol and Ammonia. In this typical response the compensated sensors show an 11% improvement discriminating ability.

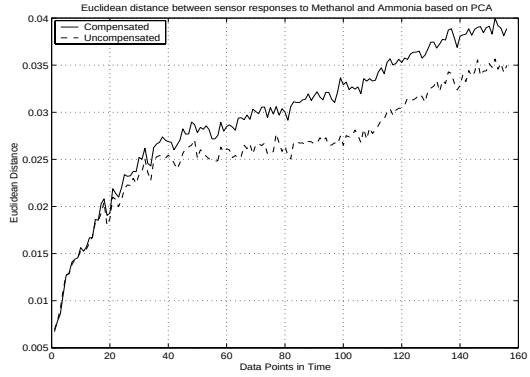

FIGURE 4-3. Principal Component Analysis on Compensated and Uncompensated Sensors

Principal component analysis is then applied to the task of using compensation to build a transient response chemical discrimination module. The primary objective of developing the chemical discrimination module is to demonstrate the transient path of a sensor to its steady-state response vector to enhance the user's ability to discriminate among analytes of interest. Visual presentation of the data is accomplished via principal component projection of the multi-dimensional sensor data; however, any data reduction system that retains salient discrimination information would be appropriate for this type of system.

After signal conditioning, the outputs of the heterogeneous arrays are transferred to a microcontroller and a principal component transformation is applied to the multi-dimensional sensor data for projection onto a portable display. Principal component analysis allows the subsequent extraction of analyte information from data in a highly efficient and compact manner. Using this type of analysis to convert the data into principal component space, the data can be displayed on a two-dimensional LCD screen. Pre-calibrated points for air and the analytes of interest are displayed on the screen as well. Users are then able to watch in real-time as the point on the screen moves in response to an applied chemical. In using a graphical display, this work takes advantage of the built-in pattern recognition abilities in the human brain to estimate that a certain analyte may be present if the data point on the screen is closer to one calibration point than others. The use of this built-in pattern recognition ability drastically reduces circuit complexity and power requirements while still supplying the needed information on chemical discrimination.

SECTION 4.5 EXPERIMENTAL RESULTS

The portable chemical discrimination system has been calibrated on multiple concentrations, up to saturation, of methanol, formaldehyde, and ammonia and tested on multiple concentrations, up to saturation, of methanol. Both tin-oxide sensor modules and mixed sensor modules have been used on demonstrate the performance of the system for these analytes.

Figure 4-4 demonstrates the results of principal component analysis, used here for analyte classification purposes. Data was taken using each of the two sensor boards described above. Calibration data is shown for each of the three analytes, formaldehyde, ammonia, and methanol. (a) and (b) represent a subsequent response to and recovery from methanol for the tin-oxide sensor board and

the mixed sensor board respectively. The path of the sensor response clearly traveled from the initial baseline area to the methanol calibration point, thereby revealing the analyte to which the module was responding. In (a) the separation between analyte clusters is well-defined. Upon recovery, the signal approaches baseline conditions. Reasons for incomplete recovery include the need for a longer recovery time, or sensor drift, which could easily be compensated using the auto-zeroing baseline compensation circuit. In (b) the analyte clusters are not very well defined. This feature illustrates an important point. The composite-film polymer chemiresistors chosen for this sensor array are not very responsive to any of the analytes chosen. This lack of response decreased the amount of variance which the principal component analysis had to work with, and thereby limit the classification ability. Large mixed sensor arrays have the potential to act as better classifiers because they can potentially be responsive to more analytes and analyte families to varying degrees, but sensor types must be chosen wisely. In both cases, a user of the module can watch as the response path approaches a cluster and using their own abilities as a classifier, make a decision as to what chemical is present.

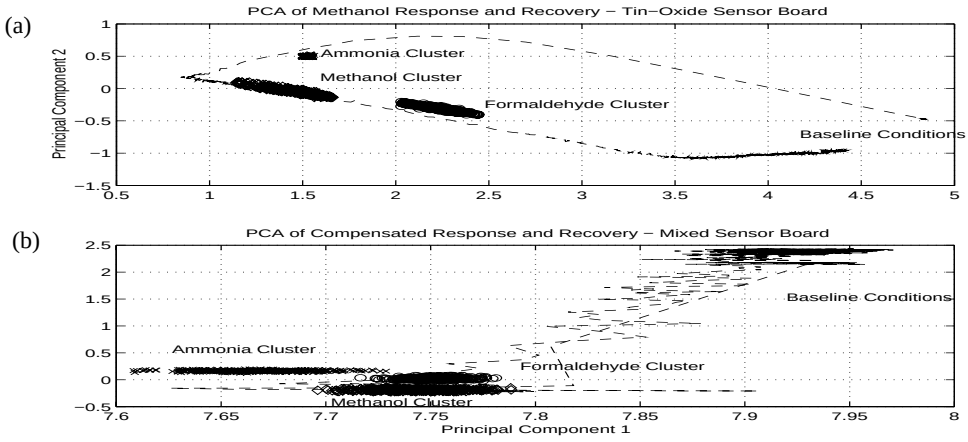

FIGURE 4-4. Principal Component Analysis Experimental Results

Figure 4-5 shows a sample display screen for the chemical module. Software features are included for resetting the compensation process, dictating when the sensors are at baseline conditions and

for starting and stopping the PCA display. In this sample screen shot, the sensor response travels

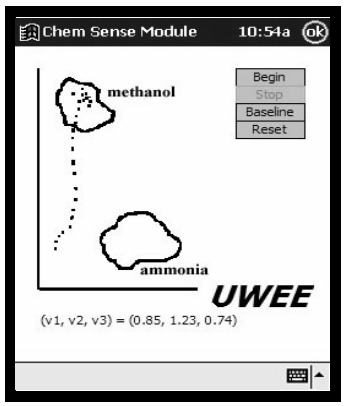

FIGURE 4-5. Sample Module Screen Shot

from initial baseline conditions to the methanol calibration cluster, which is well separated the ammonia calibration cluster. The three voltages at the bottom of the screen represent average response voltages for the three different tin-oxide sensor types. The original baseline voltage was 2V. Figure 4-6 shows the entire transient response chemical discrimination module. A small fan on the side of the box helps to deliver analyte to the sensors in a controlled manner. The entire box weighs under five pounds. Battery power enables the box to operate continuously for over two hours in the field. Three 9V Nickel Metral-Hydride battery packs are used to provide for a +18V and -9V supply for the various circuit components. The batteries have a rating of 2000 mAh.

FIGURE 4-6. Transient Response Module

SECTION 4.6 SUGGESTED FUTURE AREAS OF RESEARCH

Many areas of research could continue directly from and benefit from the work presented here. For example, future work on the compensation circuit includes adding averaging directly onto the integrated circuit, especially for the case of linearly responding sensors, to process homogenous arrays of sensors for a more robust aggregate output. Recall from Equation 2.4 that for composite polymer sensors of the same type, the constant k will be the same for each analyte for one type of sensor. The differing baseline resistance is not a factor in this equation due to the baseline compensation. Therefore, because of the linear response, independent of baseline resistance, responses of different sensors of the same type can be averaged together for a more robust response. Averaging and other statistical methods can also be used to eliminate defective sensors by comparing an individual sensor's response with the average. Finally, to further reduce noise, the signal can be averaged over time using appropriate filtering techniques. Currently, much of this averaging, filtering, and outlier removal is performed externally by digital circuitry. Optimized on-chip analog circuitry should improve performance. Converting the sensor signals to currents rather than voltages through a transduction amplifier, would put the signals in a form that are easily averaged, added, and removed as appropriate.

Another simplification beyond merely integrating the compensation circuit is to incorporate floating-gate technology in such a way that overcomes the drawbacks previously presented [12]. Currently the compensation circuit achieves baseline-compensation using an elaborately large feedback loop composed of counters, digital to analog converters and comparators. The current circuit requires that each sensor have its own complete compensation circuit. However, floating gate technology can reduce the size of the integrated compensation circuit by two orders of magnitude by using floating-gate technology as analog memory [32]. By keeping the same compensation scheme as described in previous sections, but adding analog memory, the signal will not be distorted as in previous attempts [12]. Floating gate technology will also allow most of the compensation circuit to be reused for each sensor pixel thereby further reducing size. Having a small, functional compensation circuit will enable the optimization of a large number of these chemical sensors into a small, inexpensive, low-power, mobile chemical sensor unit.

Many improvements are possible in the transient response module as well. For example, software can be improved to enable analyte calibration points to be added in the field rather than in the laboratory. Calibration points taken in the field are more accurate because they take into account field conditions such as humidity and temperature.

SECTION 4.7 SUMMARY

This research effort has described and detailed the development of the auto-zeroing baseline compensation circuit and other associated sensor signal processing such as noise filtering, outlier removal, and principle component analysis. The final integrated version of the circuit is an improvement of previous versions of the circuit in terms of accuracy, power requirements, applicability to multiple sensor types, reduced volume, and reduced cost. This circuit as designed directly compensates for variability in sensor manufacturing, sensor drift, variations in environmental parameters, and sensor poisoning, as well eliminating high-frequency sensor noise. The reduction in sensor dynamic range by this circuit has been shown to provide up to a factor of 34 improvement in response resolution for typical sensor arrangements.

Other research efforts have taken different approaches to these inherent chemical sensor problems, each with different disadvantages. For example, in the case of compensating for sensor drift, other researchers propose using a complicated combination of principal component analysis and artificial neural networks [33] or adjusting making complicated adjustments to the PCA transformation matrixes as the sensors drift over time by eliminating the first principal component [34]. The first solution has the disadvantages of adding greatly to the circuit complexity and training complexity. The second solution may not be valid, because drift may not always occur in the first two principal components and the drift direction changes depending on the history and composition of applied analytes.

Other attempts to build electronic noses have tended to use one type of sensor (e.g. only metal-oxide sensors [35] or only conducting polymer sensors [36]). In addition, these electronic noses tend to be calibrated for one specific use, such as discriminating among olive oil types [35] or monitoring aromatic hydrocarbons [36]. The compensation circuit described in this chapter along with intelligent post-processing allows for multiple sensor types to be used together in a much sim-

pler fashion than has been previously available, to the point where sensors of different types may be interchanged. Flexibility in creating sensor arrays, and the ability to compensate out deleterious sensor artifacts will lead to more general-purpose applications for electronic noses.

Experimental results have shown that baseline compensation is possible with sensors over wide manufacturing variability. Different types of compensation methods and designs have been discussed and compared, with the integrated variable current source compensator shown to have overall superior results with potential for further improvement. The integrated compensator has been shown to be able to maintain a constant current output over varying loading, with less than 0.6% deviation from a constant current with a load change of as much as 25%. Compensation to within 0.5% of desired baseline output voltages has been demonstrated using the two stage design. Drift in the current source was shown to be negligible over a period of over 24 hours. Typical sensor drift compensation results were shown in which subsequent to the sensor drifting, compensation returned the sensor to within 0.03% of the original baseline value thus preserving output dynamic range without affecting sensor sensitivity or response characteristic. Compensation to a desired baseline output for a wide range of initial sensor values was shown with an error of less than 5%. Typical results also demonstrated that the integrated compensation circuit allowed a minimum analyte detection limit twice as good as that of more traditional sensor signal extraction methods. Finally, preliminary principal component analysis demonstrates an 11% improvement in analyte discrimination ability using this compensation scheme.

Also, an interferent rejection circuit has been shown both in simulation and experiment to increase response accuracy. The circuit separates out the effect of interferents on the output compared to the response to the primary analyte.

In addition, the ability of a modular and portable chemical discrimination system to track and display response paths of multidimensional sensor arrays in principal component space has been demonstrated. The modules are designed to be low power to achieve low-power objectives and principal component analysis does not overload the low-power microcontroller (PIC 16F877) in this low-overhead system. Response paths have been shown on the module in calibration and tested to be easily identified with the human eye for three different analytes. The ability to interchange sensors of the same or different types and to compensate for unknown baseline conditions

has been demonstrated. Simple noise removal techniques and outlier removal have also been used to improve the classification ability of the module. The end result is a portable box that a user can take with them into the field to search for pre-calibrated analytes using intuitive human-oriented classification methods.

Intelligent pre-processing of chemical sensor signals have been shown to reduce the effects of sensor variability and to enhance the abilities of signal post-processing to discriminate among analytes.

References

[1] Beth C. Muñoz et al., "Conductive polymer-carbon black composites-based sensor arrays for use in an electronic nose," *Sensor Review* **19**, No. 4, pp. 300-305, 1999.

[2] D. M. Wilson, S. Hoyt, J. Janata, K. Booksh, L. Obando, "Chemical sensors for portable, handheld field instruments," *IEEE Sensors Journal* **1**, No. 4, pp. 256-274, 2001.

[3] Kousuke Ihokura and Joseph Watson, *The Stannic Oxide Gas Sensor*, pp. 49-88, CRC Press, Ann Arbor, 1994.

[4] E. Llobet et. al, "Electrical equivalent models of semiconductor gas sensors using PSPICE," *Sensors and Actuators B* **77** pp. 275-280, 2001.

[5] Janata, Jiri and Huber, Robert J., *Principles of Chemical Sensors*, pp. 152-174, Academic Press, New York, 1985.

[6] J. Janata, M. Josowicz, "Chemical Modulation of Work Function as a Transduction Mechanism for Chemical Sensors," *Accounts of Chemical Research* **31**, No. 5, pp. 241-248, 1998.

[7] Russell D. Reed and Robert J. Marks II, *Neural Smithing*, pp. 299-310, The MIT Press, Cambridge, MA, 1999.

[8] Erik J. Severin et al., "An Investigation of the Concentration Dependence and Response to Analyte Mixtures of Carbon Black/Insulating Organic Polymer Composite Vapor Detectors," *Analytical Chemistry* **72**, pp. 658-668, 2000.

[9] Mark C. Lonergan, Erik J. Severin, Brett J. Doleman, Sara A. Beaber, Robert H. Grubbs, and Nathan S. Lewis, "Array-Based Vapor Sensing Using Chemically Sensitive, Carbon-Black-Polymer Resistors," *Chemistry of Materials* **8**, No. 9, pp. 2298-2312, 1996.

[10] C. Di Natale et al., "Comparison and integration of arrays of quartz resonators and metal-oxide semiconductor chemoresistors in the quality evaluation of olive oils," *Sensors and Actuators B* **78**, pp. 303-309, 2001.

[11] J. Boris, "The threat of chemical and biological terrorism: preparing a response," *Computing in Science and Engineering* **4**, No. 2, pp. 22-32, 2002.

[12] Alyssa Apsel, Theron Stanford and Paul Hasler, "An Adaptive Front End for Olfaction," *ISCAS '98, Proceedings of the 1998 IEEE International Symposium on Circuits and Systems* **3**, pp. 107-110, 1998.

[13] J. V. Hatfield and P. I. Neaves, "A Signal Processing ASIC for an Electronic Nose," *IEE Colloquium on Application Specific Integrated Circuits for Measurement Systems*, pp. 8/1 -8/5, 1994.

[14] J. Brezmes et. al., "Application of Artificial Neural Networks to the Design and Implementation of Electronic Olfactory Systems," *NEUREL-2000, Proceedings of the 5th Seminar on Neural Network Applications in Electrical Engineering*, pp. 75-80, Belgrade, Yugoslavia, 2000.

[15] "Terra: The EOS Flagship", http://terra.nasa.gov.

[16] Sam McKennoch, D.M. Wilson, "Autoranging Compensation for Variable Baseline Chemical Sensors", *Proc. SPIE Int'l Symp. Env. Ind. Sensing*, Boston, MA, 2001.

[17] Sam McKennoch, D.M. Wilson, "Electronic Interface Modules for Solid-State Chemical Sensors", *Proc. IEEE Sensors*, Orlando, FL, 2002.

[18] Sean Hoyt, Sam McKennoch, D.M. Wilson, “Transient Response Chemical Discrimination Module”, *Proc. IEEE Sensors*, Orlando, FL, 2002.

[19] Ishnida, H., Nakamoto, T., and Moriizumi, T., “Remote sensing and localization of gas/odor source and distribution using mobile sensing system,” *Proceedings of the 1997 International Conference on Solid-State Sensors and Actuators, Transducers ‘97*, Chicago, IL, 1997.

[20] B. Lundberg and B. Sundquist, “Resistivity of a composite conducting polymer as a function of temperature, pressure, and environment: Application as a pressure and gas concentration transducer,” *Journal of Applied Physics* **60**, No. 3, pp. 1074-1079, August 1, 1986.

[21] R. D. Sherman et al., “Electron Transport Processes in Conductor-Filled Polymers,” *Polymer Engineering and Science* **23**, No. 1, pp. 36-46, 1983.

[22] B. Doleman et al., “Quantitative Study of the Resolving Power of Arrays of Carbon Black-Polymer Composites in Various-Sensing Tasks,” *Analytical Chemistry* **70**, pp. 4177-4190, 1998.

[23] John P. Uyemura, *CMOS Logic Circuit Design*, pp. 113-140, Kluwer Academic Publishers, Boston, 1999.

[24] Chao-Ming Ying and Babu Joseph, “Sensor Fault Detection Using Noise Analysis,” *Ind. Eng. Chem. Res.* **39**, No. 2, pp. 396-407, 2000.

[25] Paul R. Gray and Robert G. Meyer, *Analysis and Design of Analog Integrated Circuits*, pp. 635-667, John Wiley & Sons, Inc., New York, 1977.

[26] H. V. Shurmer, P. Corcoran, M. K. James, *Sens. Actuators B* **1993**, *16*, 256.

[27] Julian Gardner, *Microsensors: Principles and Applications*, pp. 19-30, John Wiley & Sons, Inc., New York, 1994.

[28] M. Pardo et al., “Data preprocessing enhances the classification of different brands of Espresso coffee with an electronic nose,” *Sens. Actuators B* **69**, pp. 397-403, 2000.

[29] R. Ionescu, A. Vancu, and A. Tomescu, “Time-dependant humidity calibration for drift corrections in electronic noses equipped with SnO_2 gas sensors,” *Sens. Actuators B* **69**, pp. 283-286, 2000.

[30] Denise M. Wilson and Thaddeus A. Roppel, “Hardware Architectures for Chemical Sensing Electronics,” *Proceedings of the SPIE Conference on Internal Standardization and Calibration Architectures for Chemical Sensors*, Boston, MA, 1999.

[31] Leslie M. Kay and Gilles Laurent, “Odor- and context-dependent modulation of mitral cell activity in behaving rats,” *Nature Neuroscience* **2** No. 11, pp. 1003-1009, 1999.

[32] R. R. Harrison et al., “A CMOS programmable analog memory-cell array using floating-gate circuits,” *Circuits and Systems II: Analog and Digital Signal Processing, IEEE Transactions on*, **48**, Issue 1, pp. 4-11, January 2001.

[33] M. Holmberg et al., “Drift counteraction for an electronic nose,” *Sens. Actuators B* **35/36**, pp. 528-535, 1996.

[34] A. C. Romain, Ph. Andre, and J. Nicolas, “Three year experiment with the same tin oxide sensor arrays for the identification of malodorous sources in the environment,” *Sens. Actuators B* **84**, pp. 271-277, 2002.

[35] M. Concepcion Cerrato Oliveros et al., “Electronic nose based on metal oxide semiconductor sensors as a fast alternative for the detection of adulteration of virgin olive oils,” *Analytica Chimica Acta* **459**, pp. 219-228, 2002.

[36] Joseph N. Barisci et al., "Conducting polymer sensors for monitoring aromatic hydrocarbons using an electronic nose," *Sensors and Actuators B* **84**, pp. 252-257, 2002.

Acknowledgements

The author wishes to express sincere appreciation to the following people: Dr. Nathan Lewis for providing composite-film polymer sensors; Dr. Jiri Janata and Brian Polk for providing Chem-FETs and advice on their use; Sean Hoyt for his work on the digital aspects of the transient-response chemical discrimination module; Dr. Bruce Darling for taking the time to be on my committee; all my co-workers in the DMS lab for their encouragement; Carola for the sacrifices she made to enable me to proceed through my graduate career; and my advisor Dr. Denise Wilson for providing the opportunity to undertake this effort in the first place, and for her guidance and motivation over the past two years. Without those listed above this thesis would not have been possible.